NNL Science
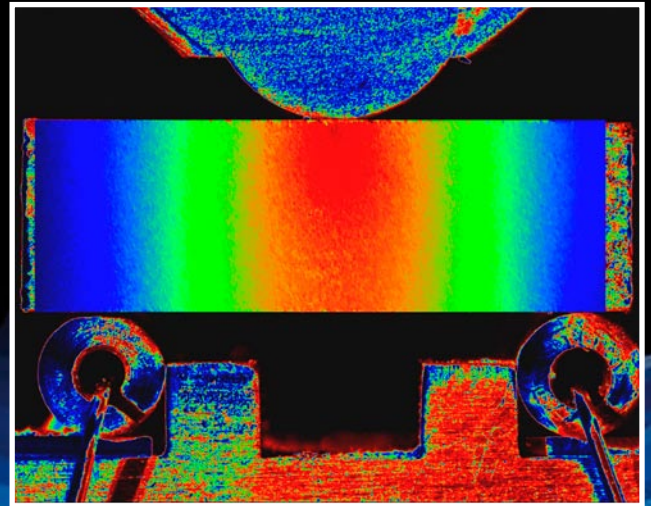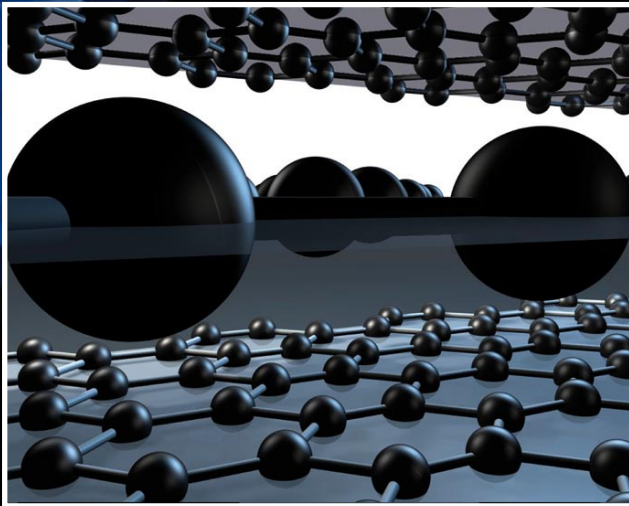
Graphite analysis using Electronic Speckle Pattern Interferometry

Also in this issue:

- **Plutonium speciation in fuel storage ponds**

- **Raman Spectroscopy of PuO_2**

- **Radiation damage in ferritic steels**

- **Development of the ENIGMA fuel performance code**

- **RADBALL - the next generation**

Contents

Introduction

Welcome to the first issue of "NNL Science".

In this journal, we present some of the many and varied pieces of peer reviewed scientific work that NNL have completed over the last year either for customers or through our own, self-funded, Signature Research programme. NNL Science illustrates the breadth and relevance of the Laboratory's work against the grand nuclear challenges of our age. It exists to stimulate scientific engagement with the NNL and therefore if you want to follow up any of the scientific work, there are contact details for the lead authors at the start of each article.

In each issue we highlight one of NNL's key capabilities. This issue focuses on the science of graphite.

Graham Fairhall
Chief Science and Technology Officer

SUPPORTING THE OPERATION AND FUTURE DECOMMISSIONING OF UK GRAPHITE MODERATED NUCLEAR PLANT

Martin Metcalfe, Nassia Tzelepi & Paul Ramsay

martin.p.metcalfe@nnl.co.uk

BACKGROUND

With the exception of Sizewell B, the United Kingdom's nuclear power generation is based on a graphite moderated gas-cooled reactor design. The original British design for a civil nuclear power plant was a carbon dioxide cooled graphite core with natural uranium fuel elements clad in magnox alloy. This design evolved and was refined as more plant were commissioned. However, due to constraints on channel gas outlet temperatures (to limit mild steel oxidation), only moderate power densities could be achieved. This was later addressed by the development of the Advanced Gas-Cooler Reactor (AGR) with a higher power density, made possible through operation at higher temperatures and gas pressures with stainless steel fuel pins containing enriched uranium oxide. The fuel pin assemblies were contained within a graphite sleeve. PGA graphite was replaced with an isotropic Gilsocarbon graphite developed to operate in this more extreme environment and manufactured from Gilsonite, a naturally-occurring form of asphalt. Over the life of the reactor, the graphite will undergo significant property changes affecting the design function of components. At the same time, radionuclides will be generated within the graphite from activation of impurities or be deposited on the graphite from the reactor gas circuits affecting future handling and disposal.
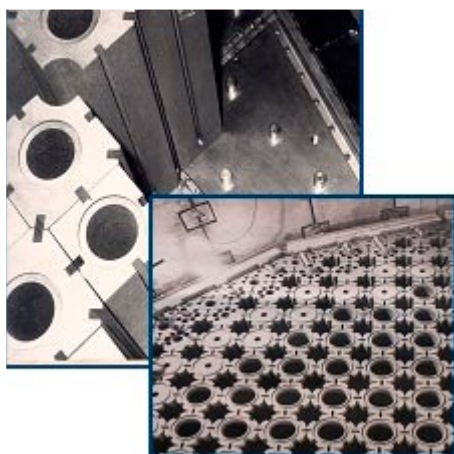

Figure 1: Interior of reactor cores shown during construction; front image AGR, rear image Magnox

Characterising and understanding the ageing of these graphites, the behaviour of individual graphite components and the behaviour of arrays of graphite components in a core has presented and continues to present a significant challenge to the plant operators. Continued safe operation of the reactors is the over-riding objective of the licensees. However, this is linked to defining the optimum lifetime, which needs to balance the generation of low carbon electricity with the gradual erosion of margin to safety case as the reactors age and degrade.

Once the plant have ceased generation, decommissioning, possible treatment and final disposal of reactor materials must eventually be undertaken.

Within the UK, there is an estimated 80,000 m^3 of irradiated graphite arising from civil nuclear plant and legacy waste (test reactors, the Windscale Piles, fuel sleeves etc.). Graphite waste management poses a significant challenge to the Nuclear Decommissioning Authority in terms of its scale, the characterisation of the potential hazard and disposal options.

NNL plays a key role in providing graphite technical support both for operating plant and for graphite waste management. It is important to acknowledge that the foundations for the NNL capability are based upon the significant contributions to graphite technology from its predecessor organisations.

NNL graphite capability

NNL offers an internationally-recognised capability in nuclear graphite that has evolved over forty years, its experience and expertise tracing back through its predecessor organisations Nexia Solutions, British Nuclear Fuels (BNFL), AEA-Technology (AEAT), United Kingdom Atomic Energy Authority (UKAEA) and the Central Electricity Generating Board (CEGB). Today, NNL is the principal provider of graphite measurements and characterisation to the UK commercial nuclear power industry, a service that is key to the continued operation of nuclear plant. In addition, NNL provides a national and international technical consultancy on nuclear graphite with interests and expertise in safety case inputs for operating nuclear plant, new build and graphite waste management. This capability is strengthened through its numerous links with universities and research organisations (e.g. US national laboratories).

Facilities and techniques

NNL operates graphite testing facilities designed to handle active material: a controlled laboratory and glove-box facility for low to medium active material and a cave facility for high active material. In addition to active material handling and sample preparation capabilities, NNL is able to provide a range of measurements on irradiated graphite including:

- Bulk density
- Helium volume
- Gas diffusivity and permeability
- Static and dynamic Young's modulus
- Compressive, flexural and tensile strength
- Coefficient of thermal expansion (CTE)
- Thermal diffusivity
- Electrical resistivity
- Rate of release of stored energy and total stored energy
- Oxidation behaviour by thermal gravimetric analysis
- Optical microscopy (bright field, fluorescent and polarised light)
- Scanning electron microscopy (SEM)
- Transmission electron microscopy (TEM)
- X-ray diffraction (XRD)
- Digital image correlation (DIC)
- Electronic speckle pattern interferometry (ESPI)
- Irradiation behaviour of graphite

NNL specialists have an in-depth understanding of the irradiation behaviour of graphite and have access to an extensive archive of experimental and operational data generated during the development of the UK gas-cooled reactor programme and collected during the operation of nuclear plant over more than 40 years. This includes investigating the relationship between microstructure and graphite properties and the dependence of dimensional change behaviour on fluence and temperature.

Support to UK operating nuclear plant

The NNL team has in-depth knowledge of Magnox and AGR graphite core designs and lifetime ageing processes and has been responsible for designing and implementing graphite core monitoring programmes to support continued operation. NNL is currently undertaking a development programme to improve existing characterisation methods and to develop new techniques, discussed below. The team has also been involved in the development of methodologies for the structural integrity assessment of cores including oxidation models and irradiation damage models, graphite properties models, analysis of the behaviour of single components and arrays of components, and the development of whole core models.

Graphite waste management

NNL is a partner in the EU-funded Carbowaste project investigating the treatment and disposal of irradiated graphite and other carbonaceous waste, undertaking reactor physics and activation modelling to predict generation of radionuclides and taking the lead on the development of an integrated waste management approach. Separate from this project, NNL has been involved in the impact behaviour of waste materials, C-14 release mechanisms and the modelling of radionuclide release into the biosphere and geosphere.

NNL internal graphite research

NNL undertakes graphite research to maintain and develop its own graphite capability, at the same time as addressing key issues facing designers of next generation gas-cooled reactors. Its graphite research programme currently includes development of novel property measurement techniques applicable to small samples, review of and investigation into the dependence of measured graphite strength on sample size, grain size and microstructure and the development of a new physically-based predictive model for polycrystalline graphite.

Graphite changes in core

Graphite properties are dependent upon the raw materials used and the method of manufacture. The manufactured product will exhibit varying degrees of within-batch variability, depending upon its type and, different batches manufactured to the same formulation will show further variability in properties. Nuclear graphite is manufactured from petroleum or pitch coke, the cokes usually being by-products of either the petroleum or the coal industry or naturally-occurring Gilsonite. After production, the cokes are purified of volatiles by high temperature calcination. The calcined coke is then graded and mixed with a suitable pitch binder. Following forming and baking, the blocks are graphitised at ~3000°C and then purified to remove metallic impurities.

The manufactured product has many nonlinear physical properties caused by the interaction between the coke particles and the binder, the generation of porosity from gas generation during calcination and the development of microcracks during cooling from the graphitisation temperature.

So graphite is a complex material with inherent variability even before it experiences a reactor environment. During reactor operation, properties change with time due to the effects of radiation.

- Fast neutron irradiation changes the atomic structure of the graphite, displacing carbon atoms to form vacancies in and interstitials between the graphene layers leading to physical, mechanical and thermal property changes.

- Radiolysis of the carbon dioxide coolant gas within the graphite pores generates chemically active species that can react with surface carbon atoms leading to mass loss and a changing microstructure. Significant weight losses can result for components in high flux positions in the core that will further modify the physical, mechanical and thermal property changes caused by fast neutron irradiation.

- Activation of impurities and transported materials deposited in the graphite pores lead to induced radioactivity. Of particular concern for eventual storage and disposal following plant decommissioning are the long half-life radionuclides carbon-14 and chlorine-36.

Inspection of UK graphite cores

The long term behaviour of graphite has been studied by experiment and subsequently monitored on operating plant since the beginnings of the UK's reactor programme. The UKAEA carried out work in material testing reactors where samples were exposed to changes of a single parameter expected within the core, for example, neutron flux, temperature, coolant and gas chemistry, to develop a series of relationships between key properties and the varying parameter.

The monitoring of graphite properties across the Magnox fleet was undertaken by the CEGB at their Berkeley facilities. Pre-characterised surveillance samples, which had been located within the reactors at start of life, were removed periodically and their physical properties measured. Similar monitoring schemes for the AGRs in England and Scotland were undertaken by the CEGB and AEAT respectively. It was later recognised that periodic withdrawal of surveillance samples did not provide sufficient data to support assessment of safe operating lifetimes for both Magnox or AGR cores and methods were designed to trepan material samples directly from the bulk core components. The task of characterising both surveillance and trepanned samples is now undertaken by NNL.

The graphite core of a gas-cooled reactor provides a structural function as well as the neutron moderation necessary to sustain a nuclear reaction. This structural function comprises location of fuel and control rods and channels for coolant gas flow. The core graphite cannot be allowed to degrade to such an extent that the fuel channels become blocked or, more importantly, the control rods cannot be inserted. The much-extended operating lifetimes of the Magnox reactors were achieved, in part, by the extensive monitoring and characterisation of the graphite cores. The degradation of the graphite in the Oldbury reactor was a factor leading to the final closure of the station. The last remaining operational Magnox reactor, Wylfa, continues to be closely monitored for graphite degradation but this is unlikely to affect the timing of its final closure. Understanding the degradation behaviour of the AGR graphite cores is equally important for the AGR fleet. Safety cases for continued operation are dependent upon ongoing monitoring and inspection and this will be reflected in the scale of sampling as lifetime extension is planned.

Although techniques are being developed to monitor *in situ* the condition of AGR bricks, there will always be a requirement to extract samples from the reactor core for property measurements under carefully controlled conditions. EDF Energy has designed equipment that trepans a cylindrical graphite specimen from a fuel channel during shutdown. The size of the trepanning equipment and the possible effects of holes in the channel walls limit the size of the trepanned specimen and consequently test samples that can be machined from it.

Although pure graphite does not become very radioactive within the reactor, the raw materials used during manufacture contain impurities which become activated by the neutron flux. The radioactive decay of these elements, cobalt, sulphur and tritium amongst others, introduces the requirement that sample machining and measurement must be carried out remotely behind radiation shielding.

The determination of mechanical properties depends on accurate measurement of distance, for example sample displacement and physical dimensions, often at the sub-micron level. Even in a non-radioactive environment such measurements can be difficult and remote operations in heavily shielded cells have needed the development of innovative equipment and methods to meet required levels of accuracy.

Routine property measurements on AGR material

Measurements undertaken by NNL on AGR samples that feed into databases for core assessments to support continued operation include bulk density, dynamic Young's modulus, coefficient of thermal expansion and flexural strength.

The density is determined by measuring the mass and volume of a sample. The volume is measured by two methods: from a volume determined from physical dimensions measured by mechanical probes and by laser triangulation methods, and from a measured open pore volume determined by helium pycnometry.

Dynamic Young's modulus is measured using an ultrasonic time of flight technique, based upon the principle that the speed of sound through a material is dependent on its Young's modulus. Using in-house designed equipment, the time taken for an ultrasonic pulse to travel through a 6 mm thick sample is measured. Given the very small time period for a pulse travelling with a velocity of 2200 m/s, a highly accurate measurement is required for reproducible results.

Coefficient of thermal expansion measurement involves the precise loading of a small sample into a dilatometer, which is capable of measuring dimensional changes of 100 nm/°C. The strength of graphite is determined from 3-point bend tests on small beams measuring around 6x6x20 mm.

New techniques

The operators of the UK power stations must demonstrate to the regulator that they understand the behaviour of the reactor cores as "end of life" approaches. The future operational state is predicted by computer models that require input data based on historical Material Test Reactor (MTR) experiments. These input data must be supported by measurements on samples trepanned from the operating reactors.

NNL continuously strives to develop new techniques or improve existing ones by investigating state of the art equipment that could provide higher speed, accuracy and reproducibility for measurements on samples with an ever-increasing range of fluence and weight loss.

Several considerations need to be taken into account when developing a new technique for measurements on irradiated graphite:

- Applicability of the technique to small and sometimes degraded samples with a very specific geometry,

- Applicability of the technique for remote operation in a radioactive cell,

- Preference for non-destructive testing so that information from a single sample can he maximised,

- Consistency with previous results or full understanding of discrepancies,

- Validation of the technique on as-manufactured and irradiated samples.

Consequently, large testing programmes are undertaken to confirm that the required levels of accuracy and reproducibility are achieved on irradiated graphite. NNL has successfully developed the following techniques for routine deployment:

- Ultrasonics for the measurement of dynamic Young's modulus (DYM),

- Laser mensuration for length and volume determinations,

- An immersion method utilising Archimedes' principle for determining bulk density,

- Three-point bend testing on very small beams to measure strength,

and investigations on behalf of EDF Energy are currently in progress to develop methods to measure:

- Electrical resistivity,

- Dynamic shear modulus,

- Work of fracture,

- An alternative method for static modulus, coupled with Poisson's ratio.

Poisson's ratio
– a technique development case study
There have been limited measurements of Poisson's ratio on irradiated graphite due to the large specimen sizes required for either static or dynamic measurements.

To measure Poisson's ratio on small irradiated specimens, NNL embarked on the development of a novel technique using modern optical interferometry.

Electronic Speckle Pattern Interferometry (ESPI) uses the speckle patterns produced by the interference of two coherent laser beams on a sample surface to measure accurate three-dimensional displacements of a target subjected to external loading. The ESPI system consists of the laser sources, a set of optics, a CCD camera and sophisticated computer processing.

NNL used its close ties with Manchester University to carry out some of the early experiments for testing the feasibility of the ESPI technique for measurement of the extremely small displacements that occur during a bend test on graphite.

The basic method for determining the elastic properties of irradiated graphite is to carry out a three point bend test using a standard geometry whilst using the ESPI camera to measure the actual beam distortions (Figure 2) as the test progresses up to the point of fracture. The displacements at certain points on the sample can be differentiated to provide a measurement of strain and the applied load can be used to determine the stress. The ratio between these numbers provides the static Young's modulus at different stress levels during the test.
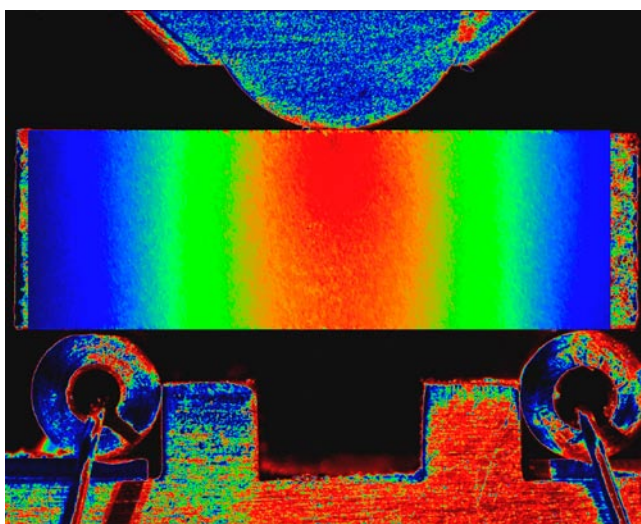

Figure 2: False colour map indicating ESPI measured displacements during a graphite three point bend test. It shows the relative Y displacements across the surface of the beam

The outcome of the study was extremely successful given the technological challenge. The ESPI technique was found to be ideal for determining the sample's local strains and hence Young's modulus but not for the original project's driver of measuring Poisson's ratio, i.e. the ratio of the strains in orthogonal directions. This was more difficult than expected, partly because the 50 nm resolution of the ESPI-measured displacements was inadequate, and partly because graphite is a granular material where the grains and binder have different properties and therefore exhibits variability within small volumes. Specifically, examination of the X displacement traces from tests on graphite showed that the majority of tests exhibited discontinuities where

the material showed extreme local strain values. These effects can be globally visualised by plotting the total X displacement array as a surface plot viewed vertically and where the surface is shaded by an oblique light source (Middle image of Figure3).

Figure 3 shows a virgin graphite sample which was tested to failure. The development of cracks can be followed within the ESPI data, culminating in the last scan at 96% of failure load (noting that only the face of the test specimen can be observed). The long crack to the right of the centreline is the path of failure, as seen in the post test image. This crack was seen to originate from the pits at the top end of the crack in the centre of the sample, and then proceeded to extend downwards as the load increased. The white trace overlaid on the surface plot shows the actual displacements along the red line on the bottom edge of the sample, scaled between +/- 15μm. The largest cracks forming to the left of the centreline, although wider, did not contribute to the sample's failure.

ESPI has also been able to demonstrate how, for virgin graphite, the measured Young's modulus is both dependent on the stress level and also on previous stress states. When a sample is first loaded up to a specific value, a permanent transformation occurs within the material so affecting Young's modulus if re-measured at any lower stress levels. Figure 4 shows a typical stress/strain curve where the applied load was cycled at increasing levels until failure. The red portion
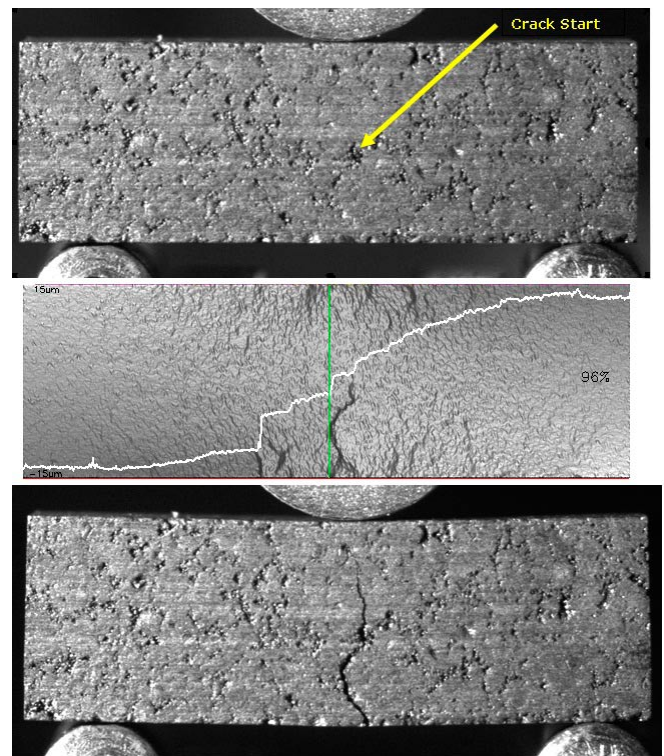

Figure 3: Images of virgin graphite sample, before (top image) and after (bottom image) testing and a shaded surface representation of measured X displacements at 96% of failure load. (The white trace shows the X displacements along the bottom edge of sample, on a +/- 15μm scale)
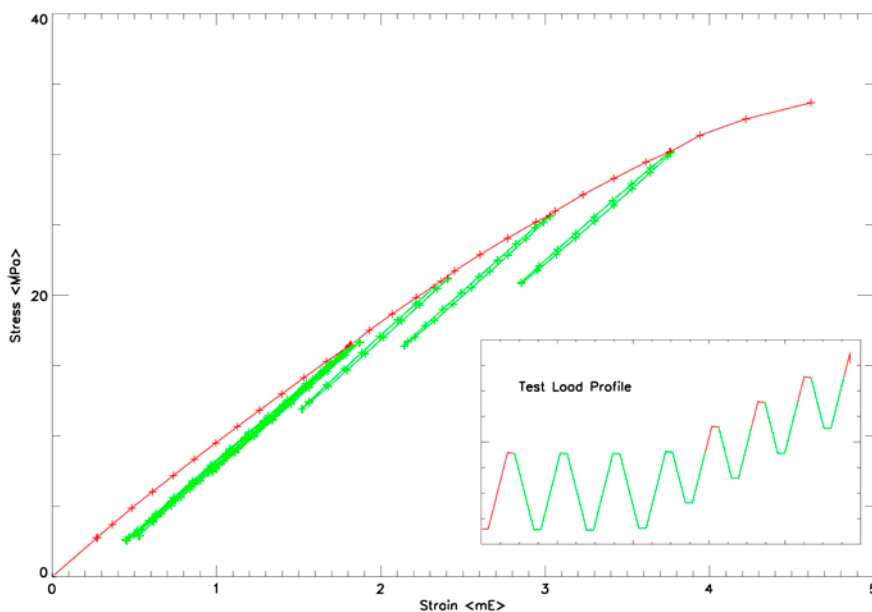

Figure 4: Stress-strain curve for virgin graphite showing the accumulation of permanent strain during repeated loading and unloading cycles

of the data indicates periods when the sample is experiencing new stress levels. This gives different instantaneous Young's modulus values compared with the green regions where the stress levels are reduced.

In Figure 5 the left-hand graph shows how the Young's modulus for virgin graphite changes depending upon the stress level of the measurement. The results have been obtained from a number of samples which have been subjected to either cyclic loading as above or a single increasing load until failure. The results have been normalised by both the modulus with respect to the Young's modulus extrapolated to a zero stress value, and the stress as a proportion of the failure stress. The graph shows that the modulus reduces linearly as the stress level increases but with two distinct gradients, with or without the permanent damage caused during first time loading, shown by the red and green data points.

The right hand graph in Figure 5 shows the same information obtained from a large programme of tests on irradiated graphite samples. In comparison with the virgin graphite, the permanent damage effect has completely disappeared and the linear reduction in modulus with stress has been replaced with nominally no change until

50% failure stress followed by a small reduction caused by the development of cracks (increasing the recorded strain). This pair of graphs clearly shows that the mechanical structure of the graphite has undergone some fundamental changes caused by the reactor environment, and understanding this mechanism and how its effect will progress into the future is the goal of the work.

The progress of this ESPI work has been presented by NNL at conferences and meetings used to disseminate worldwide experience of reactor graphite behaviour.

To further the measurement of Poisson's ratio from the ESPI displacements, a method involving Finite Element (FE) computational modelling has been developed. Various input boundary conditions to the model are adjusted whilst trying to match the model to the actual displacements of the sample under test. Following on from its experience gained in combining ESPI and computer models, NNL is taking part in a European Union funded project with the aim of providing international standards for the validation of FE computer models by making measurements on actual material by optical methods.

Currently, the ESPI technique is being further developed for measuring CTE. This could provide an independent method for measuring CTE, to supplement the existing dilatometry method.

Preparing for the future

The National Nuclear Laboratory is committed to maintaining and developing graphite technology as a key capability, both to meet the demands of its customers but also to anticipate and investigate issues that will face the nuclear industry in the future in the three areas of supporting operational plant, treating graphite waste and understanding graphite behaviour in the context of new reactor systems.
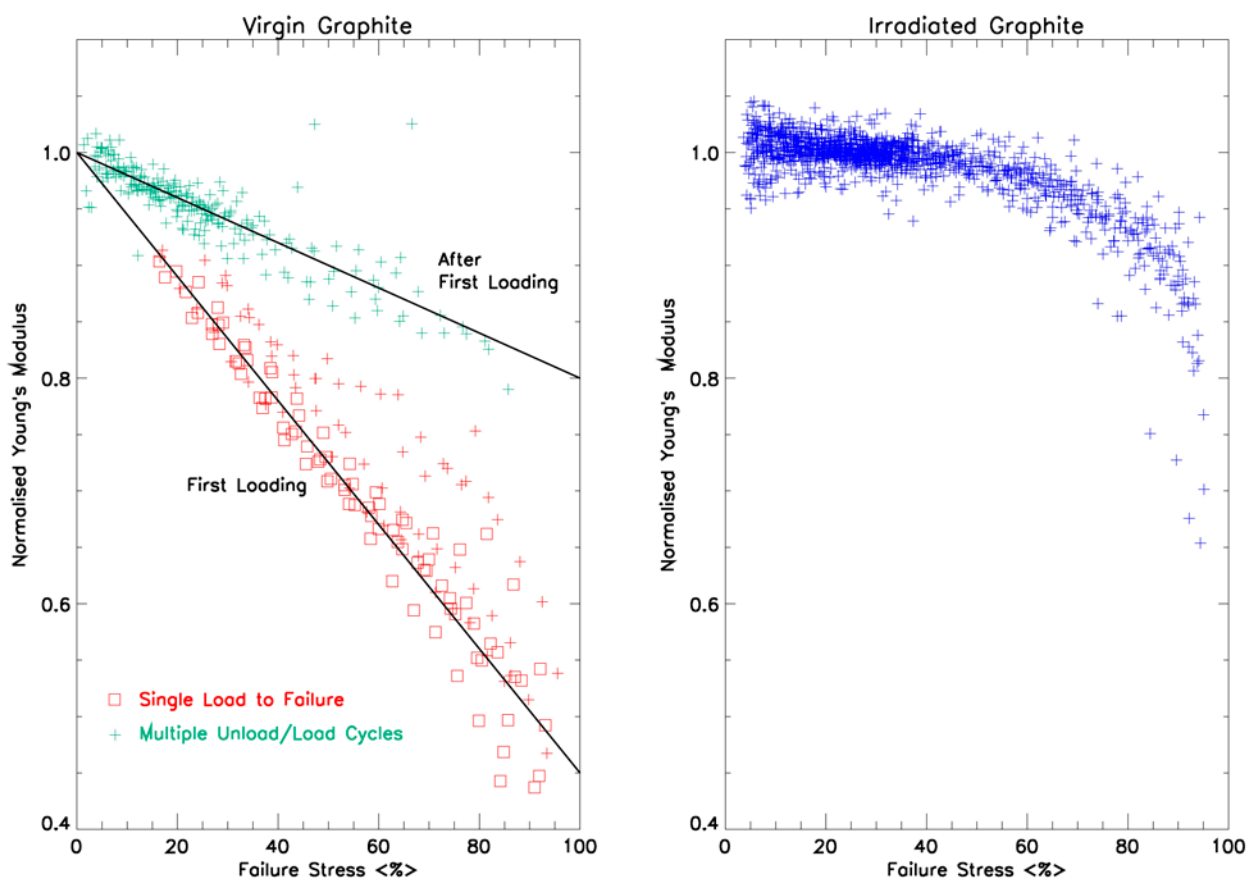
ACKNOWLEDGEMENT

Figure 5: Comparison of Young's modulus with respect to stress for graphite before and after reactor irradiation

NATIONAL NUCLEAR LABORATORY

Scientific Journal

PLUTONIUM SPECIATION IN A SELLAFIELD LEGACY FUEL STORAGE POND

Robin Taylor & Colin Gregson
robin.j.taylor@nnl.co.uk

INTRODUCTION

Within the UK there are a number of nuclear legacy fuel storage ponds and silos that contain substantial volumes of corroding spent Magnox fuel. The fuel and wastes within these ponds, including highly radioactive sludges, must be retrieved and processed during decommissioning. Sludges and other intermediate level wastes will then be encapsulated in a wasteform suitable for storage and disposal, whilst residual activity must be removed from pond liquors and process effluents prior to any authorised discharges. At Sellafield alone it is estimated that >5000 m^3 of sludge containing >10^4 TBq α-activity needs to be processed. The safe retrieval and processing of these wastes from ponds, therefore, present major engineering challenges for the UK nuclear decommissioning programme. A number of teams across NNL support these decommissioning projects and in 2004 the Waste Characterisation team took samples from a highly contaminated side bay in the 1st Generation Magnox Fuel Storage Pond during some sludge transfer trials. They subsequently developed and deployed a "Bell Jar" sampler to safely take further liquor and sludge samples from the main area of the pond (2008-9). Once standard radiochemical analysis was completed these samples presented a unique opportunity for further, more speculative, research aimed at improving our understanding of these sludges and plutonium behaviour within the ponds. Multiple chemical and physical characterisation methods were thus applied to the samples including:

- micro- and ultra- filtrations with α-spectrometry;
- Pu oxidation state analysis using indirect chemical separation methods. Two independent extraction methods were used and some additional confirmatory tests were made using alternative speciation methods on one of the samples.
- Redox potentials and pH measurements;
- Environmental scanning electron microscopy (ESEM) with Energy dispersive X-ray analysis (EDX);
- Vibrational spectroscopy (Raman and infra-red).

Pu speciation in liquor samples

The majority of the Pu-α activity was removed by filtrations of >0.2-1.0 μm with filtration at 5 μm removing a significant proportion of the activity. Once these particles were removed, the remaining activity in the Pond Bay derived samples appeared to be soluble (<1 nm). Thus there is no evidence for nano-scale Pu(OH)$_{4,am}$ based eigencolloids as are found in aqueous Pu (simulant) solutions and these data imply insoluble Pu is sorbed on to micron-scale brucite and other inorganic particles in the pond water. From Fig. 1 it can also be seen that the Pu concentrations in the filtered pond particles are significantly higher than in Pu(IV) based colloids.

The total soluble Pu concentrations are plotted in Fig. 1 as a function of pH. These data can be compared to published experimental data and theoretical solubility limits for Pu(IV) and Pu(V) species. It can be seen that Pu(V) species are dominant between pH 3 and pH 10, once colloids are removed from solution. Most interestingly, from Fig. 1 the ultrafiltered pond samples seem to show two populations. The samples from the Main Pond area (grey squares) and a downstream Holding Tank (green squares) fall as expected within the Pu(IV) solubility curve. However, soluble Pu concentrations in samples from the Pond Bay and Holding Tank following sludge transfers from the Pond Bay (red squares) seem significantly higher, falling within the range of Pu(V) solubility. Similar plots of redox potential vs. pH also indicated the same distinction between Main Pond and Pond Bay samples. Oxidation state analyses using two independent solvent extraction methods on the Pond Bay samples indicated that the soluble plutonium is predominantly present in the higher oxidation states, i.e. Pu(V)/Pu(VI). These observations were strengthened by some confirmatory tests on one sample (methods used were brucite adsorption; peroxide reduction; CaCO$_3$ co-precipitation), all of which supported the presence of oxidised Pu species in the samples. The actual solution species likely to be present under pond conditions, accounting for the role of carbonate ions present in these solutions, can be predicted using the PHREEQC speciation code and is illustrated in Fig. 2. For the samples where we have both pH and Eh we can superimpose the sample data on to this Pourbaix diagram. It is seen that the Pond Bay sample data clusters around the region of stability predicted for the Pu(V/VI) carbonate and hydroxide species whilst the Main Pond samples fall in the Pu(IV) region.
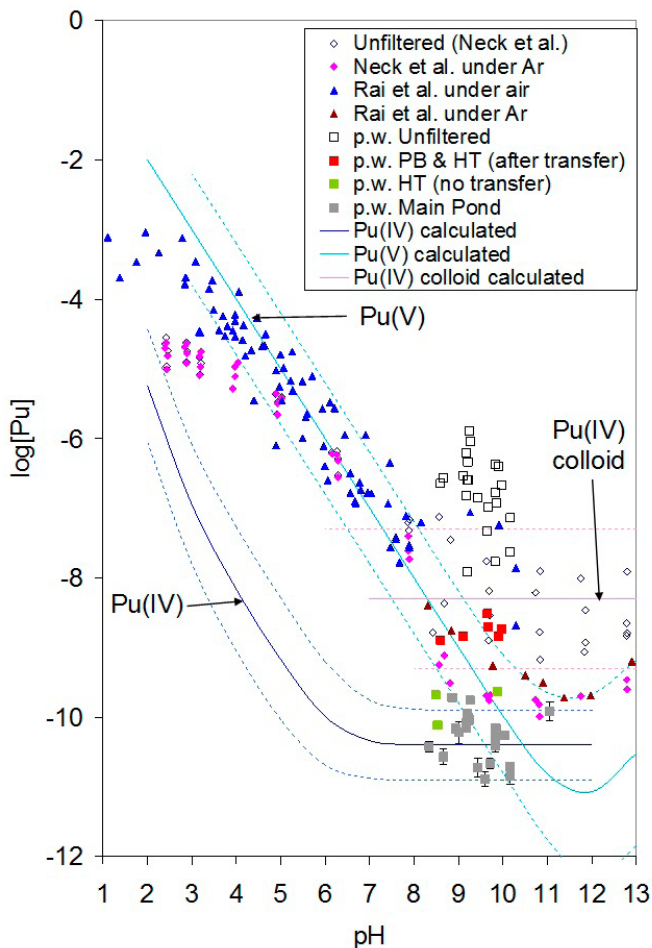
Figure 1: Compilation of molar plutonium solubilities (log scale vs. pH) showing experimental Pu data (triangles, diamonds) and theoretical solubilities for Pu(IV)$_{aq}$, Pu(V)$_{aq}$, Pu(IV)$_{colloid}$ (solid lines with associated uncertainty ranges, dashed lines) as taken from the literature. Analytical data from ultrafiltered Sellafield samples obtained in the present work (squares, "p.w.") are superimposed (green = Holding Tank; red = Pond Bay; grey = Main Pond samples). Data from unfiltered samples are given as open symbols (diamonds Pu colloids (literature data); squares = Sellafield pond samples).
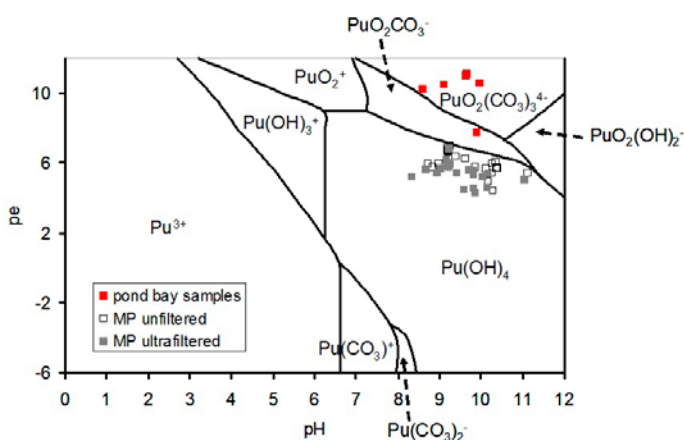

Figure 2: Plutonium Pourbaix diagram calculated using PHREEQC with Hatches database for 1 nM Pu and 10 mM CO$_3^{2-}$ concentrations. Squares indicate superimposed experimental data (colour coding same as Fig. 1)

A potential explanation for the Pu solubility and speciation data relates to pond conditions. The Main Pond is open to the air and organic materials can accumulate, thus the pond will contain dissolved organic matter, including humic acids and similar products. The Pond Bay is far less accessible being covered with concrete, circulation of water within the Main Pond is somewhat restricted (no purge) and the depth of the sludge bed is much greater (metres cf. centimetres). Organics are not thought to be a major influence within the Pond Bay. It has been shown that in the light Pu(V) is reduced by humic acid (attributed to the formation of H$_2$O$_2$). The Main Pond contains significant quantities of organic materials and is open to the air (light), Pu(IV) appears to be the dominant oxidation state in solution. The Pond Bay is isolated (dark) and suspected to contain little organic matter, Pu(V/VI) have been shown to be dominant solution oxidation states in Pond Bay samples.

Particle characterisation (filtered particles and sludge samples)

ESEM showed that suspended particles filtered from pond liquor samples were aggregates ranging in size ca. 5-25 μm and composed of clusters of interlocking platelets, 1-2 μm in size (Fig. 3a). The most common morphologies of these particles and those in the sludge samples were based on hexagonal platelets (Fig. 3b, 3c). This is quite consistent with particles imaged from corroded Magnox sludge (CMS) simulant (Fig. 3d). The obvious conclusion is that these particles are brucite, which is known to be the main Magnox corrosion product, forms hexagonal platelet crystals and has been identified as the major component of CMS simulant by X-ray diffraction. However, the high Al:Mg peak ratios observed in the EDX spectra (not shown) may be indicative of partial transformation of brucite to the closely related hydrotalcite phase, which also forms hexagonal platelets. Hydrotalcites or double layer hydroxides are a group of clays with the general formula $(M(II)_{1-x}M(III)_x(OH)_2)^{x+}(A^{n-})_{x/n}.mH_2O$ where M(II) and M(III) are di- and trivalent cations and A^{n-} is an anion to maintain charge balance.
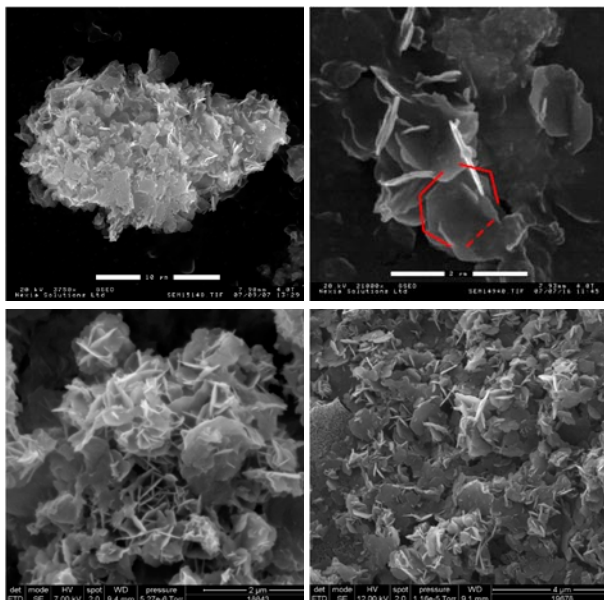
Figure 3: Examples of the predominant interlocking platelet morphology: (a) a suspended particle filtered from a Pond Bay sample; (b) expanded section, interlocking platelets clearly visible; (c) sample from the Main Pond also showing the interlocking platelet morphology; (d) CMS simulant showing similar morphology
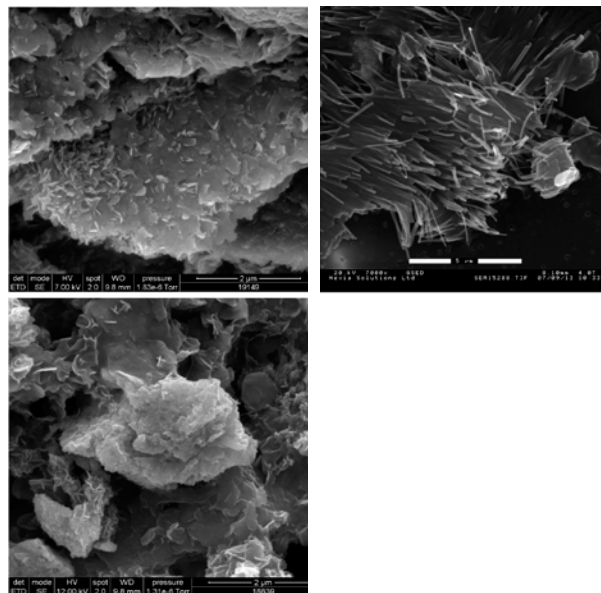

Figure 4: ESEM images: (a) secondary electron image following Au/Pd coating for Main Pond sludge sample showing corroding flake; (b) rod-like crystallites from Pond Bay sample; (c) high vacuum secondary electron image of uranium oxide particle from a Main Pond sample

Occasionally, areas of flaky material 10-20 μm were observed and on closer inspection were found to be composed of flaky sheets of closely packed platelets that differed to the more open interlocking platelet structure (Fig. 4a). EDX showed a significantly lower Al: Mg peak ratio in this area compared to neighbouring well formed platelets. This would seem to suggest that the flaky materials are pieces of cladding at earlier stages of corrosion compared to the clusters of well formed platelet crystals.

Rod or needle-like crystallites were occasionally observed in some of the suspended solids from the Pond Bay samples; in one sample large (~10 μm) clusters of crystallites were found (Fig. 4b). Rods ranged from ~1-10 μm in length and had slightly different EDX spectra with large C peaks but low Al peaks. The C peak may have been an artefact but an alternative explanation is that they are Mg-hydroxycarbonates formed from reaction between brucite and adsorbed CO_2. Some of these Mg-hydroxycarbonates (e.g. artinite, nesquehonite) have the same rod morphology and artinite has been found in simulants using X-ray diffraction. This possibility

is also supported by some evidence for CO_3^{2-} found in the Raman spectra. There was no evidence of the presence of Mg-hydroxycarbonate phases in any of the Main Pond samples (liquor or sludge samples). The conditions for transformation of brucite to artinite are probably facilitated by long term storage conditions in which CO_2 is available but ingress is restricted whilst ambient temperature conditions with high pH are maintained, conditions perhaps more like the isolated Pond Bay than the Main Pond area. Other particles were also found by ESEM, including uranium oxides from corroded Magnox fuel (Fig. 4c).

The highly fluorescent nature of all the samples and CMS simulant under Raman spectroscopic analysis was attributed to macromolecular surface-sorbed organics. The iron sulphide phase, pyrrhotite, was also found on the surface of hematite (iron oxide) particles (Fig. 5), indicative of the actions of sulphate reducing bacteria within the Main Pond area, consistent with the lower redox potentials measured in these samples.
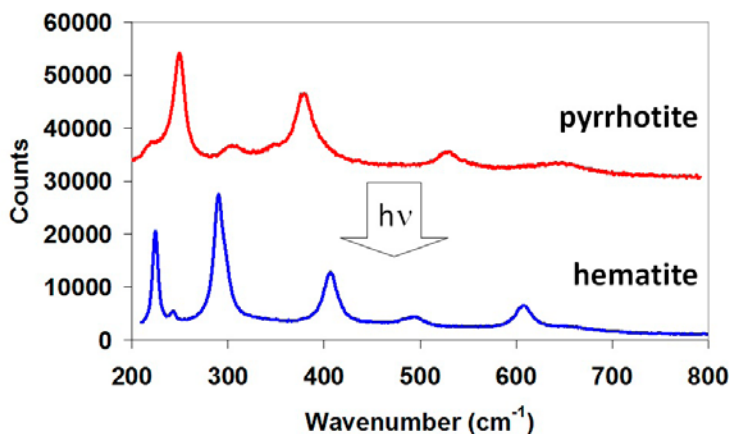

Figure 5: Micro-Raman spectra of red-brown particles from sludge sample showing pyrrhotite transforming to hematite after photo-bleaching by the Raman laser

CONCLUSIONS

These samples have presented a rare opportunity to obtain some quite unique characterisation data with the results obtained from various, independent analyses giving a remarkably consistent view of Pu speciation in the ponds. Not surprisingly, the vast majority of Pu is adsorbed onto surfaces of particles, particularly Mg particles formed from corrosion of the Magnox cladding. ESEM has been used to image these particles and most are aggregates of hexagonal platelets, expected to be brucite, although there is some evidence for partial transformation of brucite to hydrotalcite. In Pond Bay samples rods are also observed which are consistent with studies on CMS simulants that found the presence of the artinite phase. X-ray diffraction analyses of particles from different areas of the pond are now desirable to confirm the solid phases present in CMS. From size fractionation and ESEM, it seems likely that these particles will be filterable in effluent treatment.

Pu behaviour is shown to be complex due to its accessible redox chemistry with a significant fraction of Pu ions remaining in solution as truly soluble species, particularly in the samples originating from the Pond Bay. Accordingly, solution phase Pu species in Pond Bay samples are dominated by oxidised (V/VI) ions with a correspondingly higher solubility than Pu(IV) at pH 9-11, thought to be the dominant form in the Main Pond samples. These data thus point to some specific differences in chemistry between the Main Pond and Pond Bay areas consistent with differing environmental conditions.

Whilst it can not be predicted in advance exactly how such science based studies will influence future industrial operations, particularly those as complex and unprecedented as Sellafield decommissioning, a fundamental understanding of Pu speciation and solubility in UK legacy fuel storage ponds clearly extends the technical basis that underpins decommissioning of the highest hazard UK nuclear legacy facilities as well as indicating directions that can be taken to minimise soluble Pu in effluent treatment if or when required. Thus helping to ensure that clean up can be achieved efficiently and without unforeseen risks to operations or environmental discharges. For instance, by understanding the speciation of Pu in the ponds, current effluent treatment processes can be optimised and options for future processes can be proposed. Indeed, this work suggested some potentially useful methods, e.g. H_2O_2 dosing, that selectively targeted various solution phase Pu species and could be developed further if Pu polishing of effluent streams is eventually required.

Further information can be found in:

1. *Colin R. Gregson, Jeremy J. Hastings, Howard E. Sims, Helen M. Steele, and Robin J. Taylor*, Characterisation of plutonium species in alkaline liquors sampled from a UK legacy nuclear fuel storage pond, *Analytical Methods* 3, 1957-1968 (2011).

2. *Colin R. Gregson, David T. Goddard, Mark J. Sarsfield, and Robin J. Taylor,* Combined electron microscopy and vibrational spectroscopy study of corroded Magnox sludge from a legacy spent nuclear fuel storage pond, *Journal of Nuclear Materials* 412, 145-156 (2011).

RAMAN SPECTROSCOPY OF PLUTONIUM DIOXIDE

Mark Sarsfield & Helen Steele

mark.sarsfield@nnl.co.uk

INTRODUCTION

The UK has reprocessed civil spent nuclear fuel for over 50 years recovering the uranium and plutonium as products. With more than 100 tonnes of separated plutonium expected in storage the long term future of this material is being considered (1). Understanding the interactions between plutonium dioxide and constituents present during storage, such as adsorbed water and non-condensable gases, is of considerable importance to scientifically underpin continued safe storage. Raman spectroscopy has been identified as a suitable laboratory based tool to support this understanding and this paper describes the progress made in understanding the Raman spectrum of PuO_2 and how it changes with ageing.

Background

Until the 1990s the highest obtainable binary oxide of plutonium under ambient conditions was generally considered to be PuO_2. More recently there is continued debate regarding the existence of higher oxides of plutonium (PuO_{2+x} or $PuO_{2+x-y}(OH)_{2y}.zH_2O$) supported by the presence of plutonyl species with short $O=Pu^{VI/VI}=O$ interatomic distances (~1.8 Å) in reported XANES and EXAFS results. Such species have been linked to observations of hydrogen production from the reaction between PuO_2 and water vapour under certain conditions (2).

$$PuO_2 \ + \ xH_2O \ \rightarrow \ PuO_{2+x-y}(OH)_{2y}.zH_2O \ + \ H_2$$
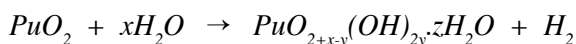
Given the reported propensity for $PuO_{2+x-y}(OH)_{2y}.zH_2O$ to exist in a range of PuO_2 materials derived from varying sources, the possibility exists that such species may form within PuO_2 originating from nuclear fuel reprocessing. Rather than using XANES and EXAFS techniques that require access to a synchrotron source that can accept plutonium samples, we considered that a

laboratory technique such as Raman spectroscopy seemed appropriate to positively identify the existence of $PuO_{2+x-y}(OH)_{2y}.zH_2O$, by identifying the uniqu Raman active vibrations of the postulated plutonyl groups $O=Pu^{V/VI}=O$.

Raman spectroscopy

Raman spectroscopy is a form of vibrational spectroscopy where light of energy sufficient can promote a molecule into a virtual excited state that then decays back to the ground state. The excitation and decay process can take 3 different routes. Rayleigh scattering is just light excited from and emitted back to the initial ground state Figure 1. Raman scattering differs from the incident radiation (ν_o) by energy that corresponds to the vibration of bonds within the molecule. The energy can be $h\nu$ less or more than the incident radiation depending on whether an increase or decrease in the vibrational energy of the molecule has occurred (Figure 1). Thus a unique fingerprint of atoms vibrating within a molecule can be identified by Raman spectroscopy.

Raman spectrum of PuO_2

Crystalline PuO_2 can be described as a face centred cubic (fcc) sublattice of Pu^{4+} ions within a simple cubic O^{2-} sublattice to form an fcc fluorite structure. Within this structure plutonium is coordinated by eight equivalent oxygen atoms at the corners of a cube, each of which is in turn surrounded by a tetrahedron of four equivalent plutonium atoms. Using group theory analysis this structure (O_h^5 point group) has a triply degenerate Raman active T_{2g} mode, a doubly degenerate F_{1u} IR active TO mode and a non-degenerate F_{1u} IR active LO mode. (TO = Transverse Optical; LO = Longitudinal Optical).

In our studies we wanted to question the existing PuO_2 vibrational frequency assignments given the possible existence of $PuO_{2+x-y}(OH)_{2y}.zH_2O$.

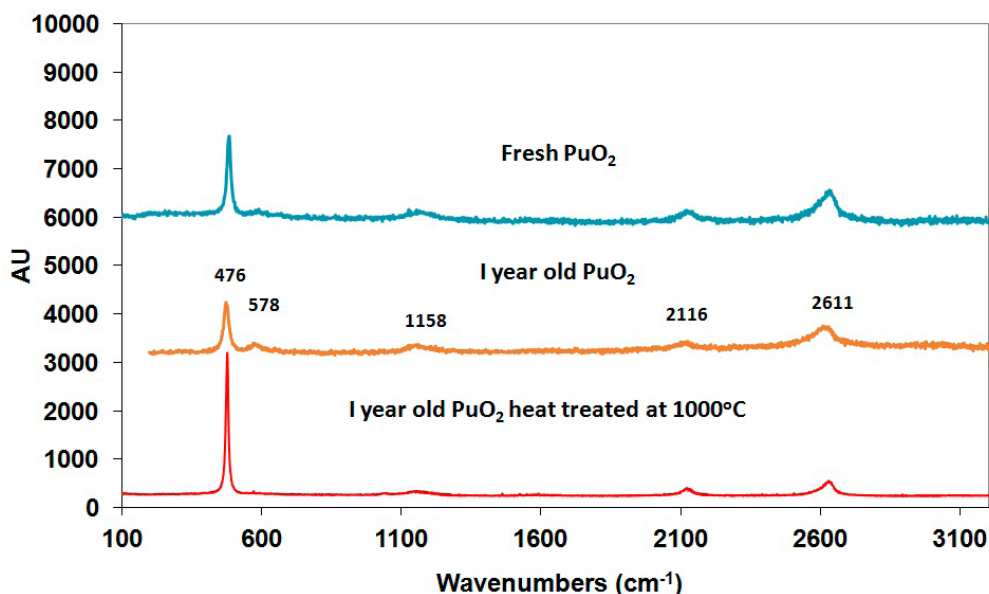**Figure 1: Vibrational energy levels of a molecule during light scattering**

Figure 2. Raman spectrum of Magnox PuO₂ (top) freshly calcined; (middle) aged for 1 year; (bottom) aged for 1 year then heated to 1000° C for 2 hrs

We examined the frequency range 200-4000 cm⁻¹ and found the Raman spectra of PuO_2 (Figure 2) to contain 5 significant signals at 476 ± 2; 578 ± 8; 1158 ± 8; 2116 ± 10 and 2611 ± 18 cm⁻¹ (errors based on an average of 11 separate samples). These samples have been examined on separate machines at two different institutes (514 nm laser – NNL; 532 nm and 633 nm laser – AWE) and the same signals exists but with slight variations in relative intensities[3].

After aging Magnox PuO_2 for more than 1 year the relative intensity of the 578 cm⁻¹ signal increases (Figure 2), whilst heating the samples to ~1000°C for 2 hours results in a relative decrease of the 578 cm⁻¹ band (compare middle and bottom plots in Figure 2).

The assignment of the 578 cm⁻¹ peak to the 1LO lattice vibration is consistent with other metal oxides with the cubic fluorite structure and most likely occurs from disorder within the structure due to either radiation defects or from amorphisation by surface hydroxide formation. However, the possibility of a higher oxide e.g. $PuO_{2+x-y}(OH)_{2y}.zH_2O$ was considered and in order to try and simulate the vibrational frequency of a

$PuO_{2+x-y}(OH)_{2y}.zH_2O$ material containing plutonyl O=Pu=O species (Scheme 1) two approaches were taken. The first approach was the gradual thermal decomposition of Pu(VI) hydroxides monitored by Raman spectroscopy to try and establish if intermediates between the hydroxides and the final dioxide could be detected.

These intermediates are expected to have a similar structure to $PuO_{2+x-y}(OH)_{2y}.zH_2O$ with plutonyl species incorporated in a mainly PuO_2 structure. Fortunately, such a decomposition mechanism is known to occur for neptunium (VI) hydroxides:

$$NpO_2(OH)_2.xH_2O \quad \rightarrow \quad Np_2O_5 \quad \rightarrow \quad NpO_2$$
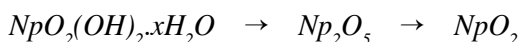
The Np_2O_5 structure contains interactions between neptunium oxo oxygens and other neptunium centres O=Np=O—Np that are similar to the interactions expected for $PuO_{2+x-y}(OH)_{2y}.zH_2O$. Comparing the decomposition routes of neptunyl and plutonyl hydroxides will provide information on whether such O=Pu=O—Pu intermediates are formed.
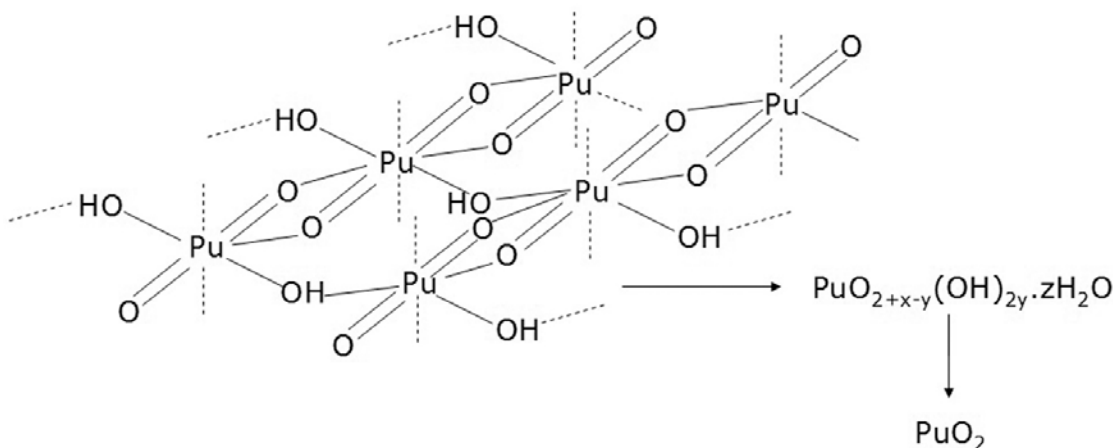
Scheme 1. Possible decomposition route of plutonyl(VI) hydroxides examined by Raman spectroscopy

The second complimentary approach involves quantum mechanical calculations of the Raman spectrum of plutonyl Pu=O oxygens bonded to other plutonium centres and compare these to the neptunyl equivalent. These calculations do not give accurate absolute vales of the Raman stretching frequencies but do provide an indication on what the difference in vibrational frequency is likely to be between isostructural neptunyl and plutonyl molecules.

Decomposition of plutonyl and neptunyl hydroxides

A sample of $PuO_2(OH)_2.xH_2O$ was decomposed using the 514 nm laser and conversion from the $O=Pu^{2+}=O$ (broad peak at 803 cm^{-1}) to what appears to be a disordered material with broad peaks at 478 and 580 cm^{-1} (Figure 4) similar to PuO_2 (Figure 2) was observed but with an additional signal, possibly due to O-H bending, at 1557 cm^{-1}. It is noteworthy that additional peaks, similar to those observed for PuO_2 at 2611 and 2116 cm^{-1}, appear as decomposition progresses.

In contrast, a sample of Np(VI) hydroxide was decomposed under the 514 nm Raman laser and was found to change from a single asymmetric Raman signal at 786 cm^{-1} to an intermediate with bands at ~ 468, 596 and 688 cm^{-1} (Figure 4). When decomposition had ceased the final Raman bands were positioned at 463, 568, 1150 cm^{-1}, as expected for NpO_2 (Figure 4). The 2LO band is assigned to 1150 cm^{-1} and is close to that of PuO_2 (1158± 8 cm^{-1}).
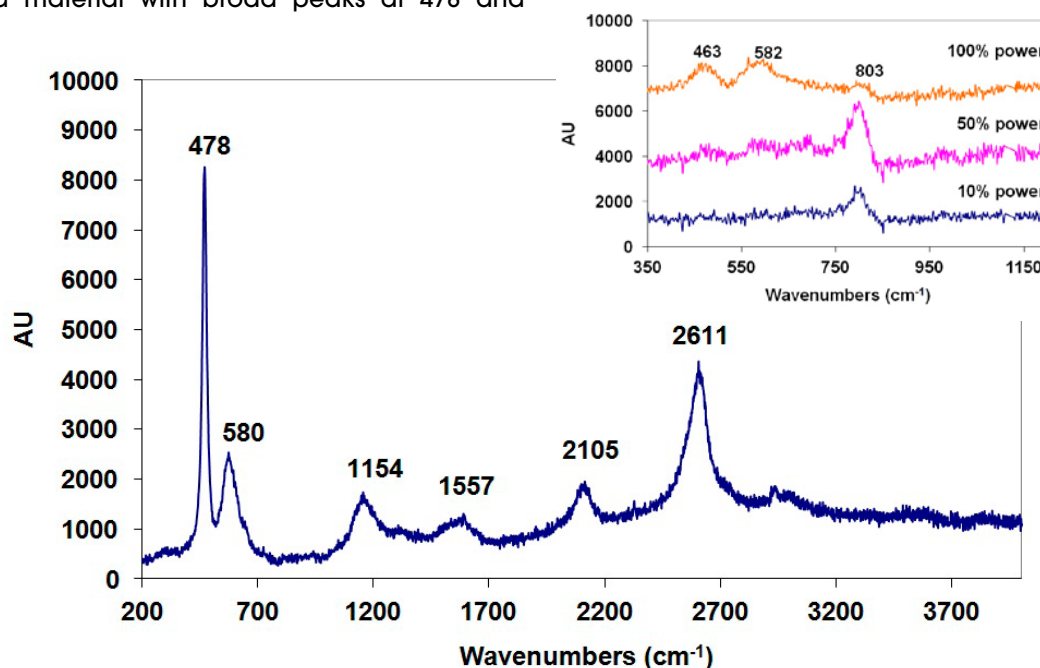

Figure 3. The full spectrum of PuO_2 created by decomposing Pu(VI) hydroxide after 2 hours irradiation with the 514 nm laser at 100 % power. (Inset) Raman spectra of Pu(VI) hydroxide decomposed under a 514 nm laser at varying power levels
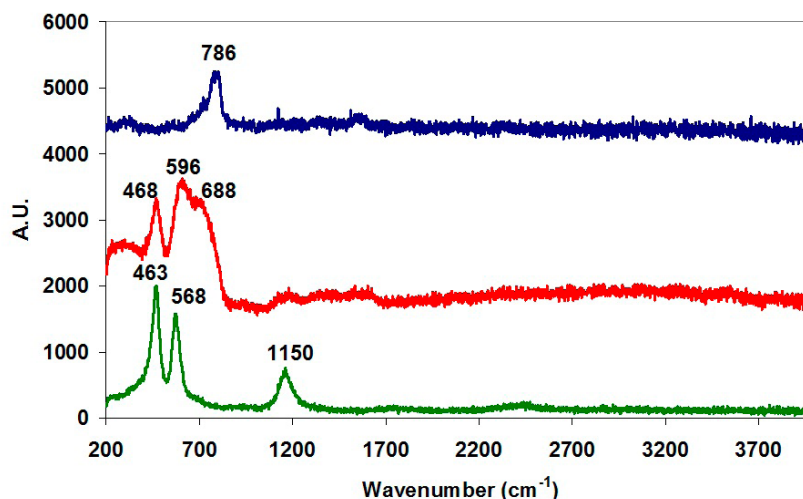

Figure 4. Raman spectrum of NpO_2 (bottom) created by decomposing $NpO_2(OH)_2$ (top) under a 514 nm laser via an intermediate compound (middle)

The decomposition of Np(VI) hydroxide by thermal gravimetric analysis involves an initial loss of water followed by Np_2O_5 formation and possibly Np_4O_9 before forming NpO_2. With more than one crystallographic Np(V) species within Np_2O_5 it is not surprising that a number of Raman bands are observed during decomposition. Note the peaks associated with the Np_2O_5 structure around 596 and 688 cm^{-1} because this is the region where $O=Pu^V=O{-}Pu$ species are to be expected within a $PuO_{2+x-y}(OH)_{2y}.zH_2O$ structure type, when in fact they are absent (see Figure 3).

Raman calculations

The Raman stretching frequency for Np and Pu molecules within a $(H_2O)_4An^+O_2{-}O=An^+=O(H_2O)_5$ type arrangement (Figure 5) was calculated using a density functional approach. The vibrational frequency difference between neptunyl and plutonyl units in $(H_2O)_4An^+O_2{-}O=An^+=O(H_2O)_5$ is small and so one would expect any plutonyl species within an oxide lattice to vibrate at a similar frequency as a neptunyl species and this is indeed what was found. For the donor plutonyl coordinating oxo group there were two symmetric stretching frequencies at 751 and 735 cm^{-1}. For the donor neptunyl coordinating oxo group these values are very similar being 746_{sym} and 735_{sym} cm^{-1}. By comparing Figures 3 (Pu) and 4 (Np) it is clear that the vibrations are not similar and that plutonyl intermediates are not formed during the decomposition of $PuO_2(OH)_2$ to PuO_2 and thus behaves differently to the decomposition of $NpO_2(OH)_2$ to NpO_2.
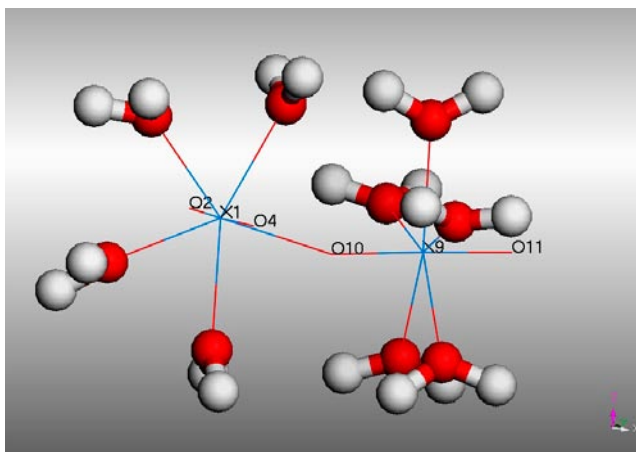
Figure 5. Structure used to model O=An=O—An interactions ($An_2O_4(H_2O)_9$; An = Np, Pu). Grey spheres = hydrogen; red spheres = oxygen; An atoms at X1 and X9 have been removed for clarity

Lattice defects

It is more likely that the 578 cm^{-1} band is a result of lattice defects due to radiation damage and the creation of vacancies and interstitial oxygens resulting in the LO band at 578 cm^{-1} becoming more allowed and thereby increasing in relative intensity. A small but measurable lattice expansion can occur due to the formation of three types of defects: anion Frenkel defects, cation Frenkel defects and defects composed of isolated helium, all as a result of alpha decay. The influence of alpha decay on the lattice parameter is well described by the empirical relationship:
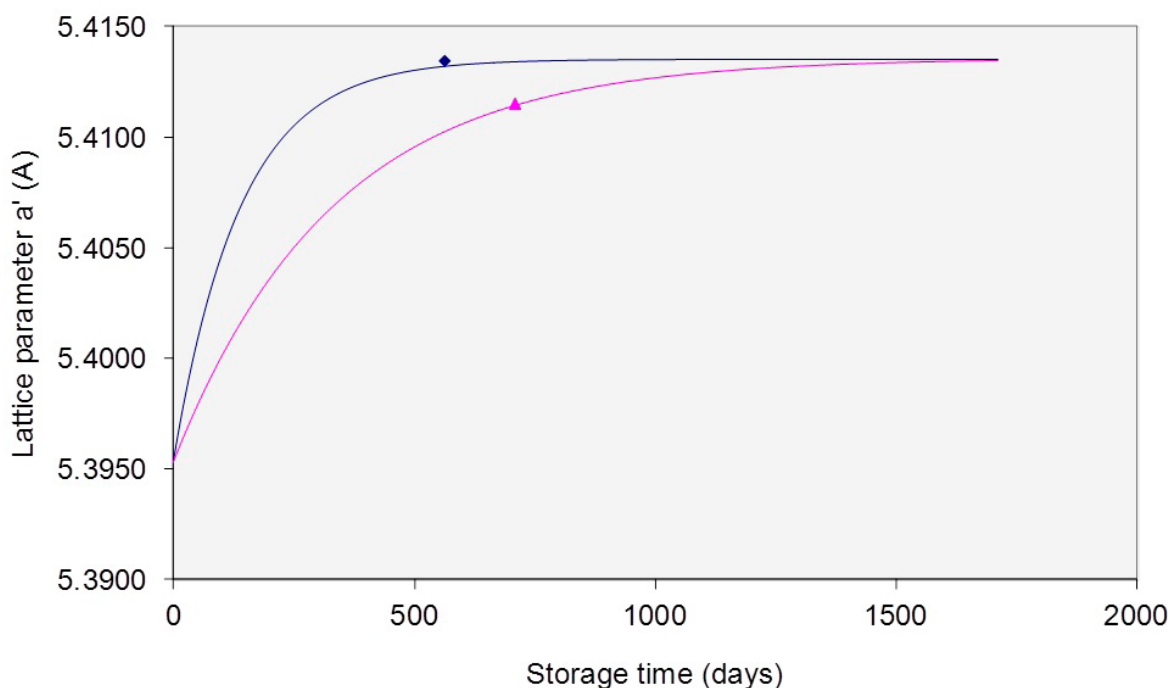
Figure 6. Calculated change in lattice parameter as a function of storage time and data points from experimentally measured PuO_2 samples (Blue = THORP PuO_2; Pink = Magnox PuO_2). Calculated curves use the empirical values A = 3.38 x 10^{-3}; B = 1.23 x10^4

NATIONAL NUCLEAR LABORATORY **Scientific Journal**

$$\frac{\Delta a}{a_o} = A \exp\{1 - (B\lambda' t)\}$$

Where Δa is the change in lattice parameter; a_0 is the lattice parameter of undamaged material; A and B are empirically derived constants; λ is the decay constant (s^{-1}); t = storage time (s). Using a weighted average decay constant λ' for the plutonium alpha emitting isotopes and ^{241}Am the expected lattice parameter value versus storage time can be plotted (Figure 6). By plotting the time elapsed from sample formation at the Sellafield reprocessing plant to the time Powder X-Ray Diffraction (PXRD) analysis was performed the expansion in lattice parameter agrees very well with the predicted value (Figure 6).

In summary, it would appear that alpha decay explains the change in lattice parameter from the expected value of 5.395(1) Å and that this is consistent with an increase in the relative intensity of the 1LO band at 578 cm^{-1} over time (Figure 1). It is the radiation damage that is responsible for the increase in intensity of the 1LO band over time and not the existence of higher oxides of plutonium such as $PuO_{2+x-y}(OH)_{2y} \cdot zH_2O$.

2LO band (1158 cm⁻¹)

In the Raman spectrum of PuO_2 a broad peak is observed near 1158 cm^{-1} similar to the band at 1150 cm^{-1} that others have assigned to the 2LO band in UO_2. This peak was initially attributed to a crystal electric field f-f transition, probably Γ^5 - Γ^3, based on calculations but some debate exists as to whether this is simply the first overtone of the 1LO band. Raman data from four MO_2 fluorite structures (M = Ce (1160 cm^{-1}), Th (1155 cm^{-1}), U (1150 cm-1), Np (1150 cm^{-1}) supports that this band generally appears in the 1150 ± 10 cm^{-1} region. This would suggest that this band is not due to crystal field electronic f-f transitions and supports the assignment of a 2LO origin.

Unassigned bands (2116 and 2611 cm⁻¹)

It has not been possible to assign the 2116 ± 10, 2611 ± 18 cm^{-1} peaks in Figure 2. They appear too low for O-H stretching vibrations from adsorption of water on the PuO_2 surface. The absorption and desorption of gases from PuO_2 has been studied by many authors (3). Gases that have been detected include: water vapour, carbon dioxide, carbon monoxide, nitric oxide, nitrogen dioxide, oxygen and nitrogen. In general, when metal oxides are exposed to the atmosphere they strongly adsorb H_2O and CO_2. Analyses of outgassing products from PuO_2 supports surface sorbed species to be: H_2O, CO_2, CO, NO, and NO_2. The strength of the major adsorbents is reported to decrease in the order $CO_2 > NO > H_2O$. The wavenumbers associated with the complexation of these molecules to the PuO_2 surface do not match the unassigned bands at 2116 and 2611

cm^{-1}. Another possible alternative would be that the 2116 and 2611 cm^{-1} Raman bands have an electronic origin associated with the electronic density of states for PuO_2 with transition energies of 262 and 324 meV respectively.

CONCLUSIONS

The use of Raman spectroscopy to analyse PuO_2 under varying storage conditions shows promise as a non destructive analytical technique and can be used to evaluate radiation damage in plutonium materials.

The Raman spectrum of PuO_2 is reported here across a wide frequency range (200-4000 cm^{-1}) for the first time and additional signals (2116 and 2611 cm^{-1}) not previously reported have been observed but are yet to be assigned with confidence. The T_{2g} signal is established at 476 ± 2 cm^{-1} in agreement with literature values. The 1LO lattice vibration is identified as a broad signal at 578 ± 8 cm^{-1} that increases in relative intensity with age. This is attributed to an increase in lattice damage with time and is supported by PXRD data. The second order Raman 2LO band is assigned to the 1158 ± 8 cm^{-1} signal and is present in MO_2 material (M = Ce, Th, U, Np, Pu), which suggests the signal does not originate from f-f electronic transitions.

The Raman spectrum of PuO_2 generated from the reprocessing of nuclear fuel has been assigned and does not support the existence of higher oxides of plutonium. Future work will examine PuO_2 exposed to conditions that favour PuO_{2+x} formation (300°C + H_2O)

Acknowledgments

References

1. NDA report - SMS/TS/B1-PLUT/001/A, "Plutonium Strategy: Current Position Paper", Feb 2011. NDA Report - SMS/TS/B1-PLUT/002/A, "Plutonium Credible Options Analysis (Gate A)", 2010
2. J.M. Haschke, T.H. Allen, L.A. Morales, *Science* **287**, 285, (2000).
3. M.J. Sarsfield, R.J. Taylor, C. Paxley, H.M. Steele, *J.Nuc Materials*, **427**, 333, (2012).
4. J.L. Stakebake, J. Nuc. Materials, **38,** 241, (1971).

RADIATION DAMAGE IN FERRITIC STEELS

Jonathan Hyde & Susan Ortner
jonathan.m.hyde@nnl.co.uk

INTRODUCTION

The effect of irradiation on reactor steels is of vital importance to nuclear power generation, especially against a backdrop of ageing plants and the desire for life extension. At present Sizewell B is the only UK commercial power plant operating with a steel reactor pressure vessel (RPV). However, safe operation of a reactor relies also on the cooling and integrity of the core, and so on many structural steel components inside an AGR or Magnox concrete pressure vessel. Worldwide there are more than 400 civil nuclear power plants and the majority of these use steel pressure vessels and all rely on steel components that are subject to neutron irradiation. Whilst radiation damage has been studied for decades, questions remain. These include how irradiated steels' characteristics are affected by alloying and impurity elements (e.g. Cu, Mn, Ni, Si, P, C, N…), microstructure or irradiation environment. Improved understanding of irradiation effects could greatly benefit future reactors and underpin life extension of the existing ones.

Irradiation damage tends to increase the strength and impair the toughness of steel, such that the mechanical properties of the pressure vessel or near-core components change throughout plant life (Figure 1). Most components must meet a minimum required toughness, which leads to temperature limits during start-up/shut-down and lifetime limitations. Degradation of toughness (i.e. embrittlement) is increasingly significant for older plant.
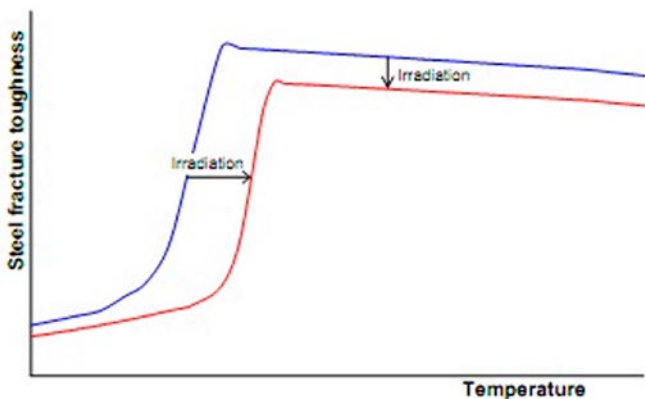
Figure 1: Schematic showing degradation of a steel's toughness as a result of neutron irradiation

Improved understanding leads to better confidence in predictions of the materials properties. It also allows for better choice of materials in the future. Data on the mechanical properties of irradiated steels are scarce. Surveillance schemes are restricted (and non-existent in case of the AGRs); experiments are expensive, limited and often impractical. Collaboration and collaborative research are therefore essential.

During the last decade, NNL has been actively researching irradiation-induced materials degradation issues. In this article, we summarise recent advances in our understanding of reactor pressure vessel embrittlement, highlighting the use of atom probe tomography (APT) and the use of models for the fracture of steels.

Reactor pressure vessel embrittlement

Extensive research on ferritic RPV steels (see, for instance (1)) has demonstrated that irradiation-induced damage can be classified as a combination of matrix damage resulting from radiation produced point defect clusters, the radiation-enhanced formation of 1–2 nm diameter clusters of atoms containing solutes such as Cu, Mn, Ni and Si, and the radiation-enhanced segregation of elements such as P to grain boundaries. Despite their very small size (2) the irradiation-induced clusters act as barriers to dislocation movement resulting in a sometimes dramatic increase in hardness and consequent embrittlement. Irradiation-induced segregation of P to grain boundaries can lead to non-

hardening embrittlement, by reducing the energy required to propagate an intergranular fracture. Using microstructural information to develop an improved mechanistic understanding of RPV embrittlement contributes to the safety cases for commercial RPVs.

Atom probe tomography (APT) of ferritic steels

Atom Probe Tomography (APT) is a rapidly advancing microstructural technique designed to characterise the 3D structure of materials with near atomic resolution. The modern microscopes provide us with the capability to characterise regions within the material of interest that are typically 50-100 nm in lateral extent and >100

nm in depth. Thus they are ideal for the characterisation of microstructures, where the features of interest are of the order of a few nanometres in size (see Figure 2). Consequently APT has been extensively used to characterise neutron irradiated steels by many different research groups world wide. Nonetheless there still remain technique-associated issues to resolve. NNL undertook a comprehensive assessment of the technique as applied to RPV steels (3) to identify and characterise potential pitfalls and artefacts. The work led to recommendations for experimental settings which provide optimised conditions for data acquisition and minimise the influence of unavoidable artefacts.
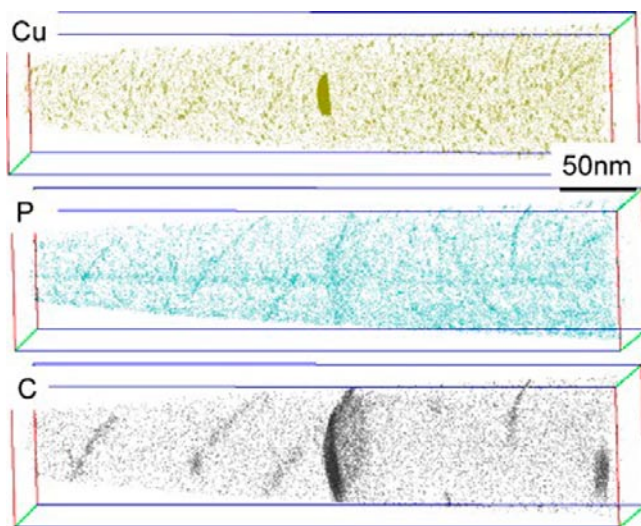
Figure 2: APT data showing nm scale clusters enriched Cu (Mn, Ni and Si), segregation of P and C to dislocations and a grain boundary, the presence of a large Cu precipitate and a carbide on the grain boundary. Each dot represents the location of an individual atom.(4)

Optimising data acquisition only covers half the battle. Unlike mature microstructural techniques such as transmission electron microscopy there are no formally approved standard methods to analyse atom probe data and even tasks that appear simple such as 'determining the composition of a precipitate' are fraught with difficulty. Working in collaboration with Rolls-Royce and the University of Oxford, NNL have been developing the most promising methodologies for characterising the size and composition of each irradiation-induced cluster. This is challenging because the 'interface' between a nanometre scale cluster and the matrix is not abrupt (Figure 3a) (2). Thus identifying which atoms belong to the cluster and which to the matrix is problematic. The approach adopted was to test cluster detection algorithms on both experimental data and modelled microstructures, whilst taking into account experimental artefacts. Good consistency was obtained comparing data obtained using an older design of atom probe (ECOPoSAP) with data from a modern atom probe (LEAP). This provides confidence that historic and new data can be directly compared. However, the analysis also showed that, for small clusters, uncertainties in defining the cluster boundaries can lead to errors in the estimation of the cluster solute content (Figure 3b) (5).
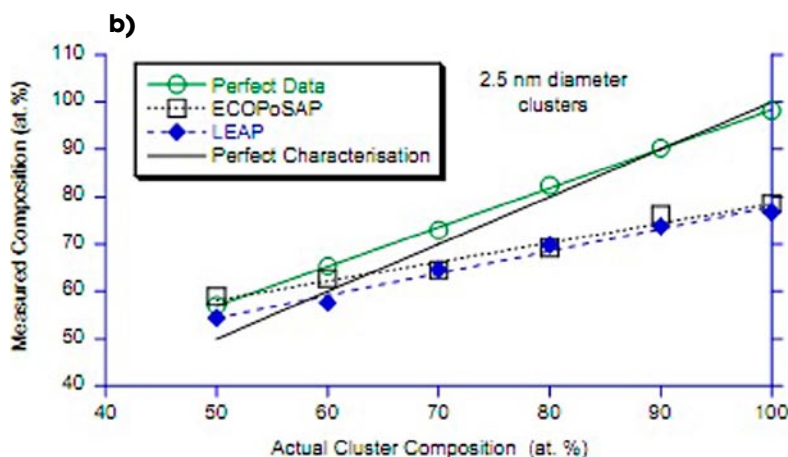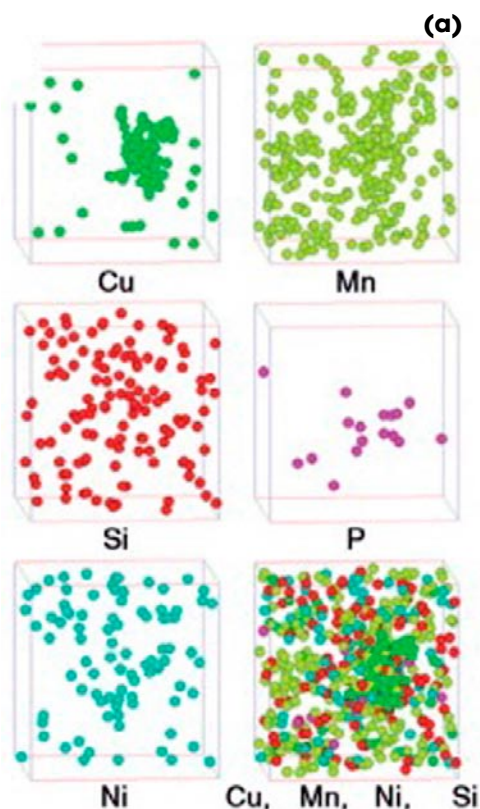
Figure 3: (a) Enlarged view of a single irradiation-induced cluster (extents of outline box 8×8×8 nm³) (2), (b) Correlation between measured cluster composition and actual cluster composition for 2.5 nm diameter clusters. (5)

Thermal ageing of RPV steels can also induce the formation of solute clusters. In contrast to neutron irradiation, the concentration of vacancies in the steel is extremely low and so the mechanism of cluster formation may differ to that in neutron irradiated RPV steels. Rolls-Royce initiated a thermal ageing program of RPV steels in ~2000. Samples of these materials have now been ageing for more than a decade at 330°C, 365°C and 405°C and during this time samples have been extracted and analysed by APT at Oxford University to monitor the level of solute precipitation. Neutron irradiated samples of these materials have also been analysed by NNL.

A detailed comparison of the structures of the clusters found in thermally aged materials and those found in the irradiated materials has now been performed (6). It was shown that clusters formed during thermal ageing have, on average, higher Cu contents and lower Mn, Ni and Si contents than those found in irradiation-induced clusters. Increasing the thermal ageing temperature resulted in a decrease in the Fe content of clusters. Despite differences in the mean compositions of clusters formed during irradiation and during thermal ageing, clusters in both exhibit similar structure. In particular, well developed clusters in both materials have Cu-enriched cores whose peripheries are enriched in Ni, Mn and, in most cases, Si. The understanding gained will help underpin future developments in Monte Carlo modelling of the precipitation processes.

Modelling predicts the formation late blooming phases (LBPs) or slowly blooming phases (SBPs) in RPV steels containing relatively high Ni. These phases are predicted to contain Mn, Ni and Si but not necessarily Cu and thus may form in modern low-Cu RPV steels. This is an increasing concern as plant operators are looking to extend plant life beyond the original design life of the RPV. Indeed this particular issue is the subject of the current EU programme "Longlife"[1]. During the last few years there has been an increasing number of observations of nanometre scale clusters containing Mn, Ni and Si in long term irradiated materials. To date it has not been possible to elucidate the mechanisms of formation from the observations or to determine their impact on material properties. Finding answers to questions such as 'Are these nanometre scale clusters irradiation-induced or irradiation-enhanced?' or 'Does the clustering represent an additional embrittlement mechanism or are the clusters a manifestation of "matrix damage"?' are areas of active research. The very long term thermally aged steels provided an opportunity to search for these features in unirradiated materials. This is a non-trivial exercise, akin to searching for a needle in a haystack, but a suitable challenge for a D. Phil. student.

It was recognised that grain boundaries are fast diffusion paths and may have heterogeneous nucleation sites for precipitation of MnNiSi features and this was, indeed, where the first ever observation in an unirradiated material was made (Figure 4) (7). The composition of Precipitates A and B are ~40Fe-32Ni-14Mn-12Si (at.%) with traces of other solutes whereas all the other clusters observed contain high Cu contents. More evidence is required before the true significance of this finding can be determined but it is an important piece of the jigsaw in our development of mechanistic understanding of degradation mechanisms in RPV steels.
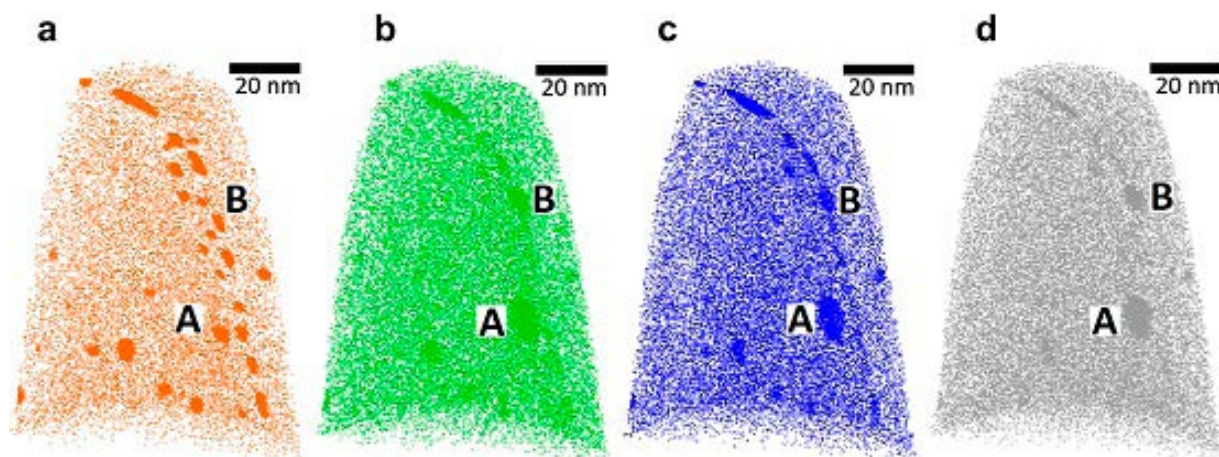

Figure 4:   Distributions of Cu, Ni, Mn and Si in precipitates at a grain boundary aged for 50,000 h at 365°C. a) Cu atoms, b) Nickel atoms, c) Manganese atoms, d) Si atoms. (7)

NATIONAL NUCLEAR LABORATORY   **Scientific Journal**

Improvements in modelling the fracture of steels

Degradation of toughness is an increasingly serious issue for older nuclear power plants. As the toughness drops, the probability of brittle failure increases. This has driven the development of models to predict toughness and relate it to changes in hardness and segregation.

A number of semi-empirical models for brittle fracture exist, including models developed within NNL (EOH) (8). Most are based on the assumption that fracture follows several stages:

- Yield occurs in the matrix, redistributing stresses and strains.
- A second-phase particle breaks, introducing a dynamic, sharp microcrack.
- The microcrack extends into the ferrite matrix without being halted by blunting in, or near, the particle: ferrite interface.
- The crack in the ferrite extends through obstacles in the matrix such as dislocation arrays and grain boundaries without blunting and arresting.

The earlier models were purely stress-based, but the more recent models incorporate strain contributions, most plausibly as an indicator of the condition required for second-phase particle cracking. This was true of the original EOH model, but some recent simulations suggest that stress x strain (W) would be more appropriate. NNL used the framework of the EOH fracture model (8) to determine whether or not the simulation predictions worked in practice. Mechanical property data from a range of different steels, including several A508 forgings and A533B plates were analysed and best fits using the EOH model obtained (9). No improvement in the descriptions of fracture toughness and initiation site properties for eight different steels over a range of temperatures was found. The use of W, however, led to the convergence of data from different steels, and to the possibility that reasonable estimates of the particle cracking criterion be made from metallographic data, even when suitable fractographic data were unavailable. Overall, experiment agreed with simulation in finding W an appropriate parameter to use to control the particle cracking stage in brittle fracture

Work carried out in association with the University of Manchester has shown the NNL fracture model to be flexible enough to incorporate the effects of residual stresses, such as are produced during plant construction (mainly welding) (10). Residual stresses were introduced by the partial loading, then unloading of a compact tension specimen. Fractographic data from specimens loaded monotonically (by a primary stress alone) or after unloading (thus by both a primary and residual stresses) were used as inputs for modelling. (An example of the particle found to have initiated fracture in a residually-stressed sample is shown in Figure 5.)
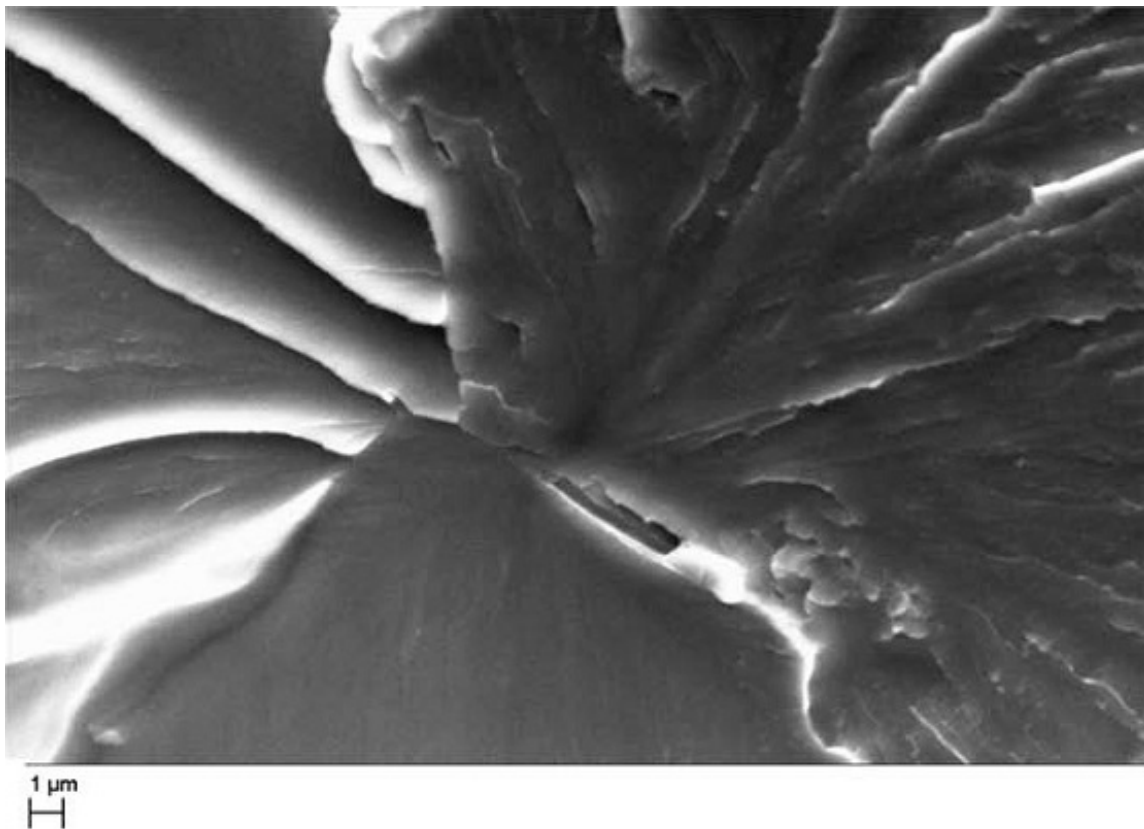

Figure 5: Broken lamellar cementite particle at site from which brittle cleavage fracture emanated in LUR sample

Three-dimensional elastic–plastic finite element calculations of the stress fields in the two types of specimen were used to characterize the stress–strain conditions at the initiation sites at the onset of brittle fracture. Use of the model made it clear that the loading which introduced the residual stress also cracked the most vulnerable particles. Subsequent unloading then induced deformation which rendered the cracked particles ineffective as cleavage nucleators during the final loading step. The critical stage in fracture therefore shifted from microcrack extension under monotonic loading conditions to particle cracking after the load-unload-reload (LUR) cycle. This produced an increase in intrinsic material toughness. The residual stress field alone increased the system constraint and reduced the primary load to failure after LUR. The use of NNL's fractography and the NNL model showed why an assessment based on the residual stress alone would be conservative.

Future prospects for characterising radiation damage by APT

APT has developed rapidly, but its true potential only becomes evident when used in conjunction with major developments in other techniques. A particularly powerful combination for studying radiation damage phenomena involves the use of ion-irradiation (which avoids activating samples thus dramatically reducing costs), Focused Ion Beam (FIB) specimen preparation (which enables pre-selection of a precise region of a material for subsequent microstructural analysis) with APT. This methodology was used to determine the effect of irradiation in the ODS-Eurofer 97 alloy (11). This material is designed as a structural material for fusion applications and is a candidate material for the blanket structures which make up part of the heat exchanger. This particular ODS steel contains Mn to scavenge sulphur. The Surrey ion-beam facility was used to irradiate the material with Fe^{2+} ions to ~2dpa at ~400° C. The use of heavy ions simulates displacement cascades caused by fast-neutron damage. Previous microstructural work on these types of steels has focused on characterising the stability of the nano-scale oxide particles. In this work the focus moved to characterising the effect of irradiation on the behaviour of multiple alloying elements. The most notable result was the dramatic segregation of Mn to dislocations following irradiation. In regions free from oxide particles the dislocation density observed was ~4 times greater than in the unirradiated material and >20 times greater than in regions of high particle density in the irradiated material. An example of the complex dislocation structure is presented in Figure 5. Compositional analyses were performed both along dislocation lines and radially from their centres so that comparisons could be made between different irradiation conditions and variations in local microstructure.

The behaviour of Mn is probably results from accelerated diffusion of solutes caused by the increase in point defects during irradiation. The relative increase in Mn to dislocations was much lower in the regions adjacent to oxide particles. The oxide particles act as trapping sites for point defects and a reduction in the point defect concentration reduces Mn diffusion. It is widely accepted that hardening in this material is caused by increasing dislocation density. The segregation found in this study could therefore act as an additional hardening mechanism as Mn pins dislocation loops. This potential effect should be considered when designing materials for fusion applications. The combination of ion irradiations, FIB specimen preparation and APT is likely to become increasingly common with the opening of the Dalton Cumbrian Facility which is currently commissioning an ion beam[2].
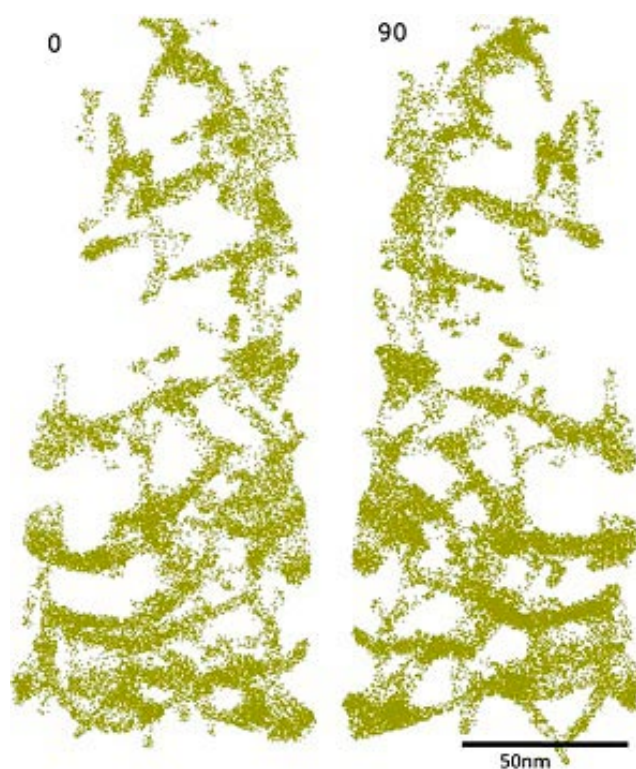

Figure 6: **ODS-Eurofer 97 irradiated to 2 dpa at 400° C. Orthogonal views of a 3D reconstruction showing Mn atoms at dislocations (No oxide particles are present in this reconstruction, and all other atoms removed for clarity). Each dot represents a Mn atom**

---

[2] http://www.dalton.manchester.ac.uk/discover/daltoncumbrianfacility/

Radiation embrittlement forum

The work summarised in this article could not have been performed without collaboration. Indeed, the need to collaborate was recognised over a decade ago when it was clear that many of the UK experts were reaching retirement age and successors were in short supply. In response EDF Energy, Magnox, ONR, RR and NNL set up the UK Radiation Embrittlement Forum (UKREF) to communicate information about international developments, to discuss topical issues and to share experience. A significant knowledge base on irradiation damage in ferritic steels has now been established and is proving useful for both successors and experts. Indeed, such is the success that the group aims to develop a parallel knowledge base covering radiation damage and thermal ageing in austenitic stainless steels. For more information contact the chairman, Dr K. Chivers at EDF Energy (katharine.chivers@edf-energy.com) or the secretary Dr J.M. Hyde (jonathan.m.hyde@nnl.co.uk).

Acknowledgements

Further information can be found in the following references:

1   **C.A. English, J.M. Hyde,** "6.08 - Radiation Embrittlement of Reactor Pressure Vessel Steels", I. Milne (Ed.) *et al.*, Comprehensive Structural Integrity, 6, Elsevier, p. 351-398, (2003).

2   **E.A. Marquis, J.M. Hyde, D.W. Saxey, S. L-P., V. de Castro, D. Hudson, C. Williams, R. Hu, S. Humphry-Baker, G. D.W. Smith,** " Atomic-scale characterisation of nuclear reactor materials", *Materials Today*, pp. 30-37, (2009).

3   **J.M. Hyde, M.G. Burke, B. Gault, D.W. Saxey, P. Styman, K.B. Wilford, T.J. Williams,** Atom probe tomography of reactor pressure vessel steels: An analysis of data integrity, *Ultramicroscopy,* 111, 676-682, (2011).

4   **E.A. Marquis and J.M. Hyde,** "Atomic Scale Analysis of Solute Behaviours by Atom-Probe Tomography", *Materials Science and Engineering Reports*, volume 69, 37-62, (2010).

5   **J.M. Hyde, E.A. Marquis, K.B. Wilford, T.J. Williams,** A sensitivity analysis of the maximum separation method for the characterisation of solute clusters, *Ultramicroscopy,* 111, 440-447, (2011).

6   **J.M. Hyde, G. Sha, E.A. Marquis, A. Morley, K.B. Wilford, T.J. Williams,** A comparison of the structure of solute clusters formed during thermal ageing and irradiation, *Ultramicroscopy* 111, 664-671, (2011).

7   **P.D. Styman, J.M. Hyde, K. Wilford, A. Morely and G.D.W. Smith,** "Precipitation in long term thermally aged high copper, high nickel model RPV steel welds", *Progress in Nuclear Energy* 57, 86-92, (2012).

8   **S. R. Ortner,** "The ductile-to-brittle transition in steels controlled by particle cracking", *Fatigue Fract. Engng. Mater. Struct.*, 29, 752–769, (2006).

9   **S.R. Ortner,** "Comparison Between Particle Cracking Criteria In Models For The Fracture Of Steels", *Fatigue Fract. Engng. Mater. Struct.*, 34, 956–973, (2011).

10 **S.R.Ortner, K.S.Lee and A.H.Sherry,** "The Effect Of A Residual Stress Field On Fracture nitiation In RPV Steel", *Fatigue Fract. Engng. Mater. Struct.*, 34, 945-955 (2011).

11 **C.A.Williams, J.M. Hyde, G.D.W. Smith and E.A. Marquis,** "Effects of heavy-ion irradiation on solute segregation to dislocations in oxide-dispersion-strengthened Eurofer 97 steel", *Journal of Nuclear Materials* 412, 100-105, (2011).

DEVELOPMENT OF THE ENIGMA COMPUTER CODE FOR SIMULATION OF THE THERMO-MECHANICAL BEHAVIOUR OF NUCLEAR FUEL RODS

Glyn Rossiter, Ian Palmer and Robert Gregg
glyn.d.rossiter@nnl.co.uk

INTRODUCTION

ENIGMA is the primary UK computer code for thermal reactor fuel performance analysis. It calculates the thermo-mechanical behaviour of a light water reactor (LWR) or advanced gas-cooled reactor (AGR) fuel rod in both steady-state and transient conditions. Versions of ENIGMA are maintained and developed by both NNL and EDF Energy - only NNL's version for LWR applications is described here. Recent development has focussed on whole core analysis and dry storage applications.

Description of ENIGMA

The coolant pressure and the irradiation history - i.e. the evolution of the axial distributions of rod power, bulk coolant temperature and fast neutron flux with time - are boundary conditions and are provided as input. Starting from the as-manufactured condition, ENIGMA then calculates the thermo-mechanical state of the fuel rod at the end of each timestep using a finite difference technique. In order to facilitate this, the active length of the fuel rod (i.e. the axial region containing the fuel
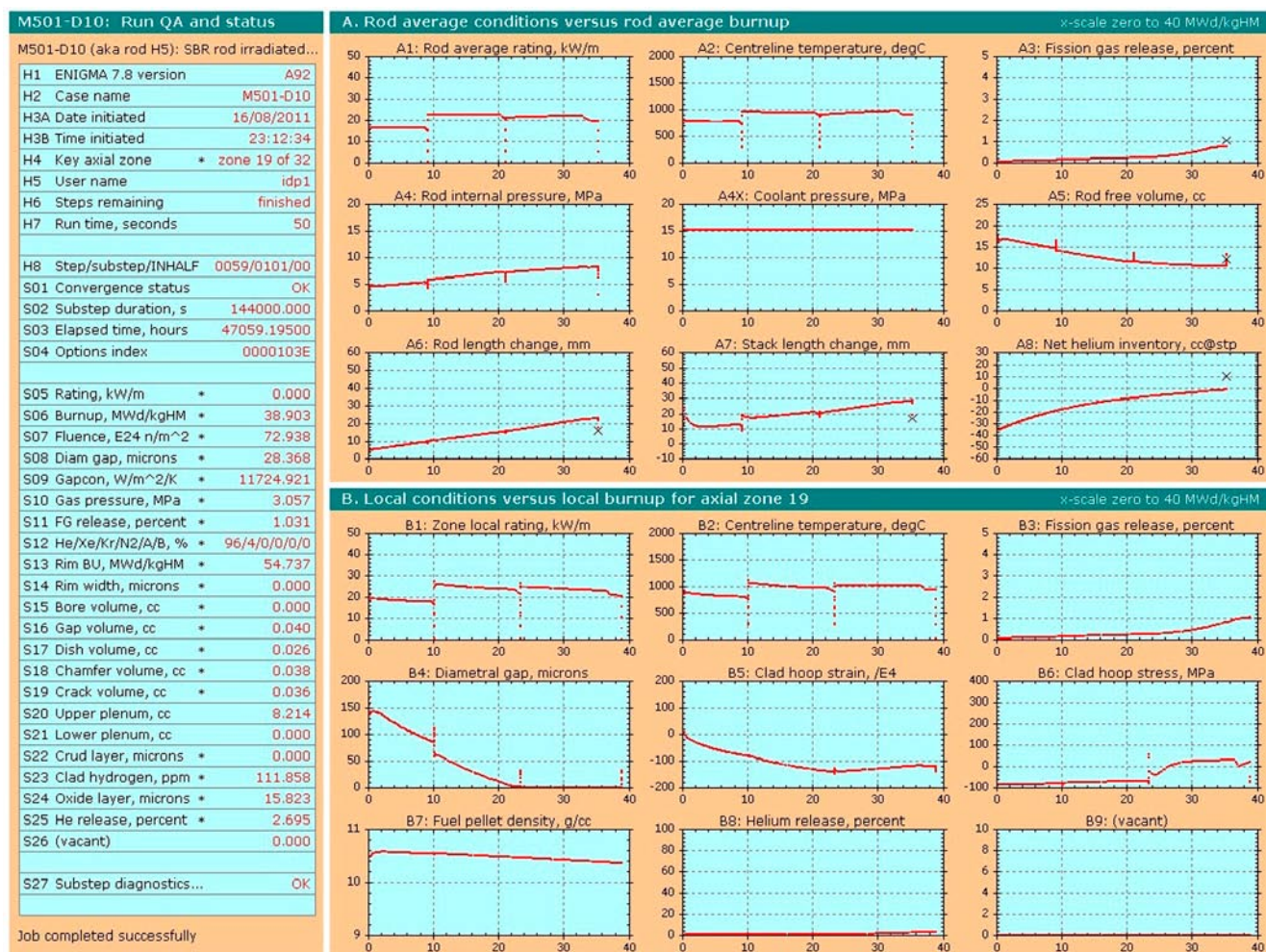

Figure 1: Example of ENIGMA screen graphics output (red lines illustrate code predictions, while black crosses show measured data)

Scientific Journal

pellets) is represented by a series of axial zones, with the fuel pellets in turn discretised into radial annuli. The free volumes associated with the fuel-clad gap, pellet dishes and chamfers, pellet cracks, the pellet bore (if any), upper plenum, and lower plenum (if any) are also modelled.

Performing the calculation described above requires the modelling of a large number of phenomena. These include: (a) standard phenomena associated with thermo-mechanical behaviour of the fuel and cladding materials, i.e. heat storage, heat transfer by conduction, convection and radiation, thermal expansion, creep, elasticity, plasticity, and fatigue; (b) phenomena related to the presence of a neutron flux, i.e. cladding hardening and axial growth; (c) phenomena related to fissioning, neutron capture and the generation of fission products in the fuel pellets, i.e. radial variation in heat generation, the generation and release of fission gas (Xe and Kr) and helium, the mixing of released fission gas and helium with the rod fill gas, and fuel densification and swelling; (d) phenomena related to microstructural changes in the fuel pellets, i.e. formation of high burnup structure and grain growth; (e) phenomena related to radial temperature gradients in the fuel pellets, i.e. pellet cracking and fuel fragment relocation, pellet wheatsheafing and clad ridging, axial extrusion and dish filling; (f) chemical phenomena, i.e. stress-corrosion cracking of the cladding, cladding oxidation, cladding hydrogen pickup, and helium adsorption by the fuel pellets.

ENIGMA is available under licence from NNL, or through Studsvik Scandpower, where it can be sub-licensed as part of their nuclear reactor analysis software suite (see http://www.studsvikscandpower.com/nuclear-reactor-analysis-software). The development version runs on a Windows PC platform, while end-user versions run on various Windows, Unix and Linux platforms. The development version includes a screen graphics capability whereby key calculated quantities (together with corresponding measured data where available) are plotted on the screen as the simulation proceeds, with results retained at the end of the run as Portable Network Graphics (PNG) files.
An example of the screen graphics output is reproduced as Figure 1.

ENIGMA is validated against a large database of LWR fuel rod irradiations in both commercial and test reactors. In total, over 500 rod irradiations with burnups up to 90 MWd/kgHM are included in the validation database. The validation system is highly automated, facilitating re-validation after any source code changes.

ENIGMA has been used for several design and licensing assessments for both UO_2 and mixed oxide (MOX) fuel, including licensing UO_2 and gadolinia-doped UO_2 in the UK Sizewell B PWR and the Finnish Loviisa VVER-440 reactor, and MOX fuel in the Swiss Beznau-1 PWR. ENIGMA is also used for analysis of experimental and commercial irradiations, for assessment of fuel behaviour during interim storage (see below), to perform feasibility studies for future irradiation scenarios, to support fuel manufacturing, and to investigate fuel failures or other fuel performance related problems.

Development of ENIGMA for whole core analysis

Historically, fuel design and licensing was generally performed by evaluating the thermo-mechanical behaviour of the limiting rod in the core with respect to each design criterion. A hypothetical bounding power history was also generally assumed, such that the power versus burnup curve for the limiting rod was an upper bound to all equivalent rod specific curves. This allowed modelling only a single rod for each design criterion analysis, and so had the advantage of minimal computation time. However, the results were subject to significant conservatism (thereby limiting plant performance and operational flexibility), the extent of which was often difficult to quantify, and for certain design criteria it was often difficult to prove that the approach taken was limiting.

The alternative of whole core fuel performance modelling, where the thermo-mechanical behaviour of every fuel rod in the core is simulated, is therefore becoming more common. This approach has the advantages of reduced conservatism (and hence more margin to design limits), more easily quantifiable uncertainties, the straightforward identification of limiting rods, and the possibility to introduce more advanced methodologies. The main disadvantage is the large amount of computing power required. However, this disadvantage is becoming less of a barrier as the available computing power inexorably increases. In particular, use of modern clusters, with parallel processing on multiple CPUs, is allowing calculations to be made that were previously not viable.

The NEXUS code has been developed by NNL to automate whole core fuel performance modelling for an LWR core, using ENIGMA as the underlying fuel performance engine. NEXUS runs on NNL's GEMSTONE high performance computing cluster (comprising ~ 250
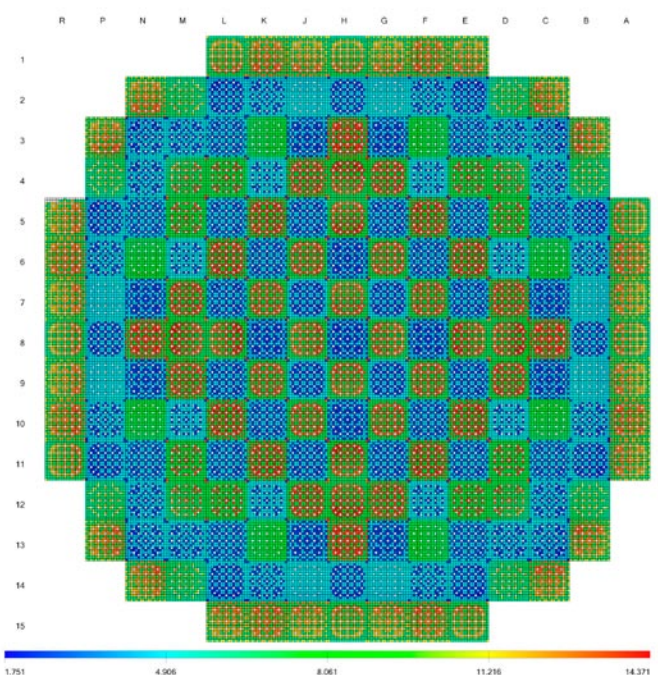

Figure 2: Sample map of ENIGMA predictions from full core NEXUS assessment: instantaneous rod internal pressure (MPa) for every rod in the core

nodes, each of which has a dual core CPU and 8 GB or more of RAM) and utilises 3-D core power distribution data obtained from the output of Studsvik Scandpower's SIMULATE code. NEXUS uses a master-slave approach, whereby a thread running on a 'master' node performs all the initial setup and distributes the ENIGMA calculational workload across accessible GEMSTONE 'slave' nodes. The slaves 'listen' for calls from the master node to begin an ENIGMA calculation. Once a call is made and all the necessary data are passed, the slave performs the ENIGMA calculation and when complete informs the master by returning a success/error code. The master-slave communication utilises the Message Passing Interface (MPI) protocol.

Visualisation of ENIGMA's rod-by-rod fuel performance parameter predictions is possible with a data viewing tool specifically designed to deal with the vast amount of data generated in a full core NEXUS assessment. The visualisation tool generates pin-by-pin 2D maps of user-specified fuel performance parameters on a total rod, rod average, user-specified elevation, maximum local (peak node), or minimum local basis (as appropriate for the parameter of interest). Maps can be of either instantaneous, minimum through-life, or maximum through-life values. An example map of instantaneous rod internal pressure is illustrated in Figure 2.

Using only 24 nodes on the GEMSTONE cluster, a NEXUS analysis of a 193 assembly (four loop) PWR core of 17x17 fuel (~ 51,000 fuel rods) takes only ~ 10 minutes, compared to more than 24 hours if the individual ENIGMA runs were executed on a desktop PC.

NEXUS analyses have been performed as part of two customer projects: plutonium disposition studies for the UK Nuclear Decommissioning Authority (see reference 3 under "Further information" below); and analysis of an operational event in one of Southern Nuclear Operating Company's PWRs (in co-operation with Studsvik Scandpower - see reference 4 under "Further information" below). In the first project NEXUS was used in stand-alone mode, while in the second it was used within the ONUS on-line fuel performance surveillance framework.

A NEXUS whole core fuel performance assessment can give the evolution with time (or burnup) of any fuel performance parameter of interest at every axial elevation (where applicable) for every rod in a given core. The parameters of interest include fuel centreline temperature, rod internal pressure, clad hoop strain, stress-corrosion crack length and clad hoop stress.

Development of ENIGMA for dry storage assessments

There is an ongoing need for site licence companies and utilities to develop and implement detailed plans for the disposition of spent nuclear fuel, and for regulators to approve these plans. The disposition could include reprocessing, storage (both interim and long-term) and/or final disposal. There are also handling and transport issues associated with these options. With this in mind, NNL have developed ENIGMA for modelling dry storage scenarios (including analysis of the pre-storage drying process). The ENIGMA modelling sits within a broader NNL framework for dry storage simulation which includes: calculation of previous irradiation history using Studsvik Scandpower's nuclear reactor analysis software suite; calculation of the decay heat output, and the actinide, fission product and activation product inventory of the spent fuel using the FISPIN code; calculation of clad temperatures during pond cooling, fuel assembly drying and/or storage using in-house and commercial thermal analysis / computational fluid dynamics (CFD) codes (including the ANSYS FLUENT software).

The relatively high clad temperatures and high rod internal pressures during drying and dry storage result in permanent creep deformation of the cladding over time. The creep strains can be enhanced in cladding with substantial metal loss due to significant in-pile clad oxidation. The dominant clad failure mechanism during dry storage (at least for zirconium-alloy clad LWR fuel) is therefore creep rupture. Severe embrittlement or delayed hydride cracking as a result of the formation of radial hydrides can also lead to clad failure, and are major concerns. Hence, the primary aim of ENIGMA analysis is to predict whether or not the cladding could fail via these mechanisms. This is done by comparing the clad hoop stresses, clad creep hoop strains and clad temperatures that are predicted during the post-irradiation operations to safety limits. (Thus, radial hydride formation is not modelled explicitly - instead the clad hoop stress is shown to be maintained below a safety limit which precludes the formation of radial hydrides.)

In order to achieve the above, ENIGMA has been developed such that it can model the thermo-mechanical behaviour of a given LWR fuel rod during irradiation, pond cooling, drying, and dry storage (assuming the fuel rod has not failed during irradiation). This involved: (a) incorporating an out-of-pile clad creep model for irradiated Zircaloy-4 (discussed further below); (b) including the ability to simulate annealing out of the clad irradiation damage; (c) writing of additional post-irradiation output; (d) several other minor modifications to allow modelling of post-irradiation conditions, including suppression of clad corrosion modelling, optional use of in-pile or out-of-pile clad creep correlations for the post-irradiation operation, optional application of a multiplier to the fission gas diffusion coefficient to facilitate investigating the effects of uncertainties on fission gas release on post-irradiation behaviour, and changes to the format of times in the main output to cater for simulated operation over 100 years and more. The ability to vary the rod external pressure from in-reactor conditions (typically 15.5 MPa for a PWR, or 7.5 MPa for a BWR) to pond cooling conditions (atmospheric plus a hydrostatic component), to drying conditions (zero for vacuum drying), to dry storage conditions (typically ~ 7 bar) was adapted from the already existing capability for modelling reactor changes.

The out-of-pile clad creep model for irradiated Zircaloy-4 that was implemented in ENIGMA is based on the creep formulation developed by Bouffioux et al (Proc. 8th International Conference on Radioactive Waste Management and Environmental Remediation

(ICEM'01), Bruges, Belgium, 30 September - 4 October 2001), since this is cited by several independent organisations as the best available model for dry storage applications.

ENIGMA dry storage assessments (for storage times of up to 100 years) have been performed for spent UO_2 and MOX fuel from both existing PWRs and new build units. Sample output from one of these assessments (3.9 year cooled UO_2 fuel irradiated in a commercial PWR to an assembly average burnup of 47 MWd/kgU) is illustrated in Figure 3, where, in this case, drying was ignored. The time is the elapsed time since the start of irradiation. 'Maximum' is with respect to axial variations (not time).

SUMMARY

NNL's version of the ENIGMA fuel performance code for LWR applications is a state-of-the-art tool for simulation of the thermo-mechanical behaviour of LWR fuel. NNL are working with Studsvik Scandpower to allow international access to ENIGMA via licence agreements.

The recent development of ENIGMA has focussed on whole core analysis and dry storage applications. With respect to the former, the NEXUS code has been developed by NNL to automate whole core fuel performance modelling for an LWR core, using ENIGMA as the underlying fuel performance engine. With respect to the latter, ENIGMA has been developed such that it can model the thermo-mechanical behaviour of a given LWR fuel rod during irradiation, pond cooling, drying, and dry storage.

The whole core analysis and dry storage applications development is part of a broader ENIGMA maintenance and development programme at NNL; this broader programme includes validation database updating, model development and capability enhancement (in areas including fuel design and licensing, whole core modelling, spent fuel storage and final disposal applications, fuel surveillance, and analysis of severe transients) and is informed by customer feedback and participation in international programmes (including the OECD Halden Reactor Project and the IAEA FUMEX-III co-ordinated research project). The ENIGMA development programme is itself directed by NNL's Signature Research Programme for internally funded R&D.
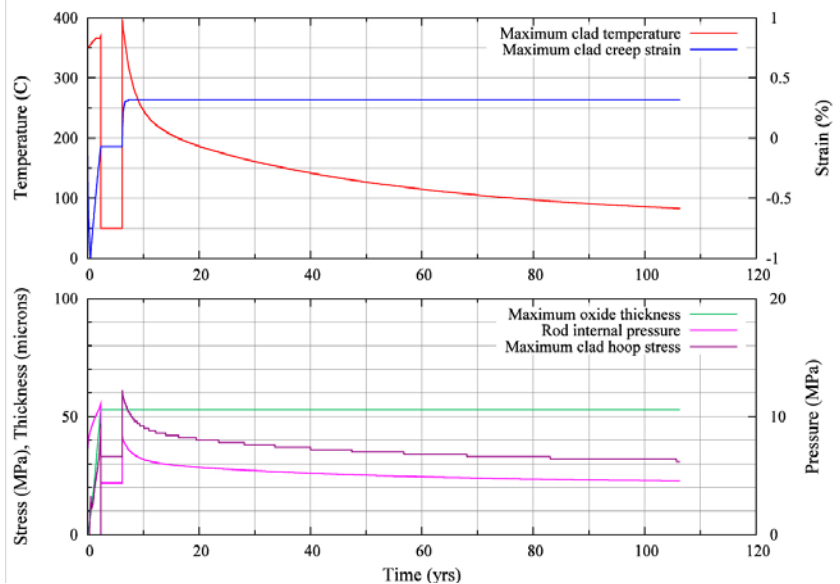
Figure 3: Sample output from ENIGMA dry storage assessment (3.9 year cooled UO_2 fuel irradiated in a commercial PWR to an assembly average burnup of 47 MWd/kgU)

Further information can be found in:

1. *G. Rossiter,* "Development of the ENIGMA fuel performance code for whole core analysis and dry storage assessments", Nuclear Engineering and Technology Vol. 43 No. 6 (2011).

2. *A. Worrall and A. S. DiGiovine,* "ONUS: on-line fuel performance surveillance - linking Studsvik's CMS with UK NNL's ENIGMA-B", Proc. Advances in Nuclear Fuel Management IV (ANFM 2009), Hilton Head Island, South Carolina, USA (2009).

3. *A. Worrall, T. J. Abram, R. W. H. Gregg, K. W. Hesketh, I. D. Palmer, G. D. Rossiter and G. M. Thomas,* "Plutonium utilization options in future UK PWRs using MOX and inert matrix fuels", Proc. Global 2007, Boise, Idaho, USA (2007).

4. *A. Alapour, R. M. Joyce, A. S. DiGiovine, S. Tarves, N. Patino, A. Worrall, R. Gregg and G. Rossiter,* "Robust PCI monitoring during PWR operation at Southern Nuclear", Proc. 2010 LWR Fuel Performance/TopFuel/WRFPM, Orlando, Florida, USA (2010).

THE DEVELOPMENT AND TESTING OF A MUCH IMPROVED RADBALL®:
A SMALL DEPLOYABLE 360° VIEW RADIATION HOT-SPOT IMAGING DEVICE

Steven Stanley & Kat Lennox
steven.j.stanley@nnl.co.uk

INTRODUCTION

The RadBall® is a 140 mm (5½") diameter deployable, passive, non electrical gamma hot-spot imaging device that offers a 360° view of the deployment area. The device is particularly useful in instances where the radiation fields inside a nuclear facility are unknown but required in order to plan a suitable decommissioning strategy. The original version of the technology had a number of drawbacks including a relative intensity to radiation (at least 3 Gy required) which led to long deployment times as well as a narrow target dose range (3 and 8 Gy) which meant that the user required a prior knowledge of the radiation fields in which the device was to be deployed. The UK's National Nuclear Laboratory have now developed the technology to overcome both of these issues. The developments associated with the new technology are described here as well as some recent tests undertaken at the Sellafield facility in the UK. The work has resulted in a significant improvement in sensitivity of x150 as well as much widened target dose range of between 20 mGy to 50 Gy. The new version of the technology therefore has a much improved applicability compared to the original technology.

The original RadBall®

The original RadBall® is a novel, passive radiation mapping device invented and developed by the UK's National Nuclear Laboratory (NNL). It consists of a truncated sphere of radiochromic polymer encased within a spherical tungsten collimation device. The collimator preferentially allows gamma radiation through the holes which interact with the polymer and causes a change in optical density (darkening). The polymer can then be scanned using an optical 3D Computed Tomography system. The darkening appears as tracks within the polymer which can be extrapolated to locate the sources and intensities of radiation within the deployment area. The original version of the technology requires a target dose of between 3 and 8 Gy and therefore is not suitable for low dose environments. Also, because the target dose range is relatively narrow the user required some knowledge of the radiation fields within the deployment area prior to the actual deployment. Furthermore, the polymer is temperature sensitive making absolute dose assessments challenging for environments with raised temperatures. To increase the market potential of the technology, some development work has been undertaken to create a newer and much improved version of the technology. This report summarises this development work and subsequent testing.

Aims and objectives

The primary objective of this project was to create a version of the technology which could detect radiation hot spots which were too low for the original technology to detect. In addition it was desirable to significantly widen the target dose range for the technology in order to move away from the situation where 'a prior' information is required regarding the radiation levels and more towards being able to use the technology 'in anger' with very little knowledge of the given radiation levels. A further supplementary aim of the development work was to offer better stability to elevated temperature. Therefore, once the new version of the technology was created further aims and objectives included the testing of the device for low dose applications, development of analysis technique as well as to undertake a number of real life trials on the UK's Sellafield site with like for like dose rate comparisons.

The new RadBall® device

The new device consists, as with the original device, of two constituent parts (as seen in Figure 1), an inner core which fits inside the tungsten outer collimation sheath. As before the outside diameter of the device is 140 mm (approx 5 ½ inch) which allows deployment in to hard to reach areas whilst providing a 360° view of the area. The inner core of new device has been based upon replicating a 3D dosimeter using 2D slices of film which can be encased in the original collimator. This was achieved by designing an assembly which holds alternating layers of film and aluminium slices. The film and aluminium slices are circular and therefore by altering the diameter of the slices a truncated sphere can be created of the same size as the original 3D polymer based dosimeter.
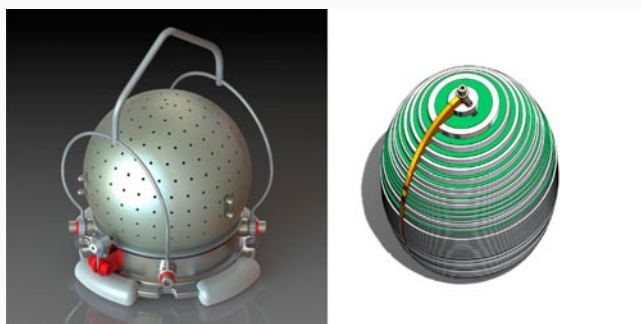

Figure 1: (left) the new inner core assembly made up of stacked sheets and slices and (right) the collimation device with lifting handle, collar and base plate

The aforementioned assembly has been designed so that the slices of film are in a known orientation and they have been laser marked to outline the order of stacking. The Gafchromic® film which makes up the layers is EBT2 film which has a very wide dynamic range with a sensitivity range down to around 0.02 Gy up to 50 Gy and is also stable in temperature up to 50°C. Therefore, one can provide an estimate of the required deployment times for varying approximate dose rates as shown in Table I. The layers of aluminium between the films are of varying thickness to ensure coverage of all incident angles of radiation without the amount of film within the device being unworkable for scanning purposes.

Table I – Estimate of the required deployment times for varying approximate dose rates

Dose Rate at RadBall	Range of Deployment Time
1 mGy hr[1]	2 days – 1 year
10 mGy hr[1]	5 hours – 0.5 year
100 mGy hr[1]	30 minutes – 2 weeks
1 Gy hr[1]	3 minutes – 40 hours
10 Gy hr[1]	20 seconds – 4 hours
100 Gy hr[1]	1 second – 30 minutes

The RadBall® service

The overall radiation mapping service based on the device consists of six individual steps. Step 1 involves placing the device inside the given contaminated area with a known position and orientation. This can be achieved in a number of ways including deployment by crane, robot, by an operator or (as in most cases) by a remotely operated manipulator arm. Once the device has been placed in position, Step 2 involves leaving the device in-situ to enable dose uptake. Once the device has been left in-situ and has achieved a suitable dose uptake (between 20 mGy and 50 Gy), Step 3 involves removing the device from the contaminated area. Usually the device has been tripled bagged prior to deployment to safeguard against contamination so this step usually involves removing the aforementioned bags. Once Health Physics clearance has been given, Step 4 involves removing the radiation sensitive core from within the collimation, ensuring that it has not rotated or moved during the deployment period.

Step 5 involves scanning the radiation sensitive sheets within the device using a specially designed scanning template on a flatbed optical scanner. The scanning template aligns each layer within the devices for analysis purposes. Minor modifications to the data removal process and data sheet were needed to make the new data sets compatible with the original software to enable subsequent analysis. This consisted of taking the series of 2D scans of the slices of film and creating a 3D block of data. When creating this block of data, each scan in the set was repeated 3 or 5 times to enhance its side on view (see Figure 2) to aid track analysis. To represent the geometric configuration of the slices in the core, the aluminium slices were made up of black pixels. The data removal process was altered to only extract the data from each track (i.e. not the black voxels).
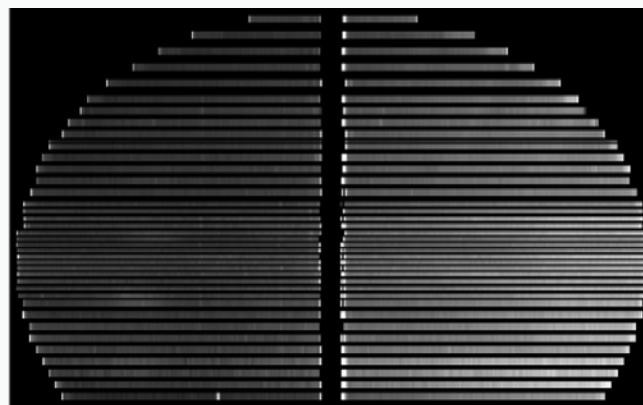

Figure 2: Side view of sliced type data set typical of the new version

Once the radiation sensitive film layers have been scanned and digitised, Step 6 involves the interpretation of this data set to produce a final visualisation. 'ImageJ' is used for the direct visualisation of the scan results in the form of a stack of 2D images after which the data from the areas of interest (radiation tracks) is extracted and exported as a list of coordinates and corresponding intensities. Once all data points have been converted to a universal coordinate system a data file is created in the correct format to be readable by the NNL's RadBall® Tool software. This consists of a number of tabs, specifically named, which hold information such as the track data, the mark point (used to align the polymer co-ordinate system with the global co-ordinate system), the vector the orientation mark, the size and shape of the deployment volume and the location and orientation of the device within the deployment volume. The first tab is used to view the deployment area and the location of the device within the deployment area, as shown in Figure 3 (left). The second tab, as shown in Figure 3 (right) is used to view the data points of all the tracks within the irradiated polymer.
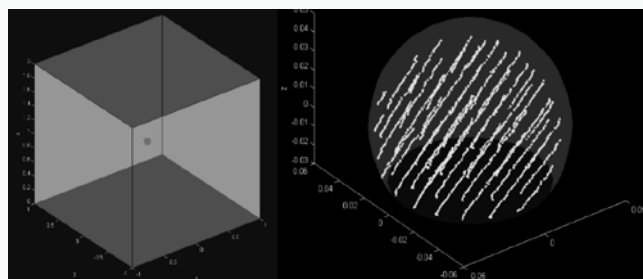
Figure 3: Screen shots from visualisation software package

For each track within the irradiated film set, the software creates a line of best fit for the data points provided and chooses the direction of the track by using the intensity values. This line of best fit is extrapolated until it intersects with a wall of the deployment volume. This indicates that the radiation source is on the wall at this location or anywhere along the line of site between the device and the point on the wall. If two devices are deployed in different locations within the same deployment area, triangulation can be used to predict where along the extrapolated line the radiation source is.

The third and final tab within the software is used to view the predicted radiation source locations. The software also has an image export function that exports each wall of the deployment area as a separate image. Each wall consists of a standard background colour and areas of colour change, which represent locations of radiation sources. This area of colour change is a Gaussian distribution about the extrapolated track intersection point on the wall. Higher intensity tracks within the device relate to brighter areas of colour change. If more than one Gaussian overlaps, each has a weighted Gaussian calculated (by intensity) and the overlapped area is a summation of the weighted Gaussian distributions.

The final stage of the analysis involves creating a file which provides a visual representation of the deployment area. This file clearly shows the locations of the radiation sources. Google SketchUp™ is a freeware visualisation tool that can be used to quickly and easily create rooms and buildings. A room is created which has the same dimensions as the deployment volume and key features such as tables or large objects can be included. Google SketchUp™ has a 2D import function which allows images or photographs to be placed within the room that has been created. This function is used to paste each wall that was exported from the software into the representation of the deployment area. Images can be layered so it is very useful to add any photographs from the deployment area to create a more realistic and useful representation of the deployment area and associated radiation sources. Moreover, delivering the final results in this way enables the customer a means to interact with their particular data set using freeware 3D visualisation software.

In field results

A shielded cell on the Sellafield Site, UK, was identified as a suitable on plant test. The radiation levels within this particular shielded cell were suitable for man entry with limited working times. This allowed the easy deployment of the technology and tested the applicability of the technology in facilities with radiation level low enough to allow limited man entry. The information received up front for the deployments were minimal and therefore the deployments represented a true blind test likeness to a real life deployment. Detail of the size and shape of the area was given as well as an old photo of the area for clarity which was used to choose the location of the deployments. A deployment plan for each of the three irradiations was created which included deployment instructions and location information.

The third deployment plan was created after the results from the first two deployments were analysed so as to triangulate the maximum number of sources. Figure 4 shows a slice of film from the first two deployments as well as associated Google SketchUp visualisations showing the directional predictions for each detected source.
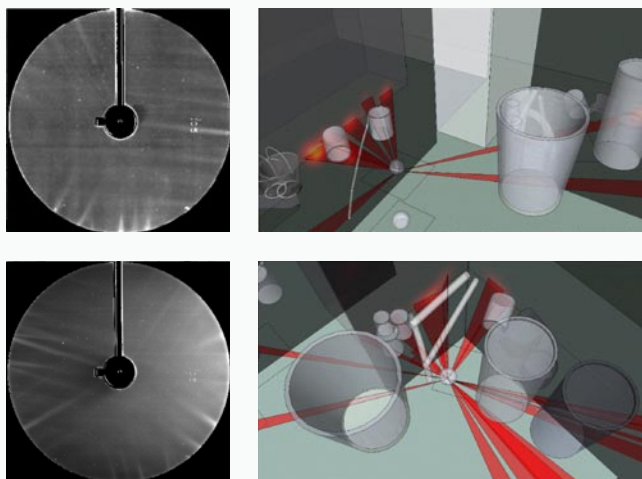
Figure 4: (left) processed image of a film slice and (right) Google SketchUp output predicting source direction for the first (top) and second (bottom) deployments

Figure 5 shows the final results with full triangulation of sources found by the new technology. The sources have been numbered in the figure 6. The deployment locations are shown as D1, D2 and D3; sources are numbered; distributed low energy gamma sources are lettered A and B; and independent measurement locations displayed as X, Y and Z. The corresponding information shown in Table IV show the resultant dose rates provided as equivalent doses at 0.1 m from the source.

Figure 5: Final triangulated results from all three deployments showing source locations

Within Figure 6, there are also points labelled X, Y and Z. These are the locations or sources where data was able to be obtained via an independent health physics survey. An un-collimated RO-20 ion chamber survey device was used to obtain these measurements. Although there is some directionality in the RO-20 device, these measurements provide a point measurement. True source dose rates for comparison are not able to be provided as the background in the cell and nearby sources will always contribute to the dose rate for an un-collimated device.

NATIONAL NUCLEAR LABORATORY

Accuracy of RadBall® results

Figure 6 and Table III shows three manual and independent point dose rate measurements (X, Y and Z) taken from a survey of the area using an un-collimated RO-20 device. After these three measurements were made, the individual taking the measurement had to leave due to dose constraints which meant that further dose rate points were not able to be obtained. Additionally, it was decided that the previous survey of the area was conducted too long ago and therefore the data was not relevant due to changes to the area to draw any meaningful conclusions. As such, the 3 data points obtained were used for the comparison with the device. Point X in Figure 6 and Table III gave a reading of 35.0 mGy hr[1] gamma (approximately contact) to the container shown in the figure. The device tested predicted that the source was actually adjacent to this container with a dose rate of between 36.5 and 40.3 mGy hr[1] at 10cm which shows a reasonable level of agreement between the two radiation measurement methodologies. Point Y should give a good indication of the dose rate of Source 10. Source 10 was measured at 17.1 mGy hr[1] (at 10cm) by deployment 2 and Point Y was measured at 18.0 mGy hr[1] (contact) which again shows a very positive agreement between dose rate measurement techniques. Point Z indicates that there was a tin which is a 2.8 mGy hr[1] gamma source which was not located by the device. Calculations show that with a dose rate of 2.8 mGy hr[1] gamma, all the device locations were too far away to locate this source as the total dose received by the film over the deployment time would be lower than the detectable amount. However, should the third deployment have been positioned as intended, this source would most likely have been located as the total dose delivered to the film would have been > 20 mGy. As such, it is important to provide a limit of detection plan in future to ensure that the customer expectations are managed.

CONCLUSIONS

The main conclusion of this report is the applicability of the new version of the technology as a viable technology to be used for radiation mapping and dose assessment. The technology has seen an increased in sensitivity of around 150 times with a minimum total dose response rate of around 20 mGy. The technology has proven itself to be an early information tool for optioneering within the waste management and decommissioning sector. It could be used either in hard to reach areas, highly active areas or within man entry cells as an alternative to a health physics survey.

The film chosen has a large dynamic range, so as where this report has focused on the lower end of the films range, its higher end extends to around 50 Gy. Within the highly active or difficult to reach areas, the technology provides a versatile solution to obtaining source location and dose rate information (even at temperature) where other technologies struggle due to size, contamination and the presence of electronic components. Using the technology rather than health physics survey can provide a significant dose saving to an individual. Additionally, the technology can

determine between source and shine and therefore false positives are not likely to occur.

Table IV: Summary of dose rate results collected using the device and the RO-20 device

Source Number	Dose Rate Prediction (mGy hr[1])	Comments
1	36.5 – 40.3	-
2	1.1 and 3.8	Two sources within this tin
3	0.5 – 1.9	Container moved between deployments
4	0.2 – 2.4 – 3.7	Dose rate from different angles different suggests source is distributed.
5	1.0 – 1.7	-
6a	5.5	-
6b	1.9	-
7	1.7	-
8	0.9	-
9	15.0 – 22.4	-
10	17.1	-
11	12.3	-
A	0.1 – 0.3	-
B	0.5	-
Independent Measurement	Dose Rate Prediction (mGy hr[1])	Comments
X	35.0	This was measured at contact
Y	18.0	This was measured at contact.
Z	2.8	This was measured at contact.

Further information can be found in:

1. **S.J Stanley,** Nuclear Future., 4(6), 302-308 (2008).

2. **E.B. Farfán, S.J. Stanley, C.J. Holmes, K. Lennox, M. Oldham, C. Clift, J. Adamovics**, Health Phys. 102, 196-207 (2012).

3. **S.J. Stanley, K. Lennox, E.B. Farfán, R.J. Coleman, J. Adamovics, A. Thomas, M. Oldham,** J. Radiol. Prot. 32, 131-145 (2012).

OTHER TECHNICAL NEWS

Pu Futures Summer School

The 2012 Actinet Plutonium Futures Summer School was hosted by the UK National Nuclear Laboratory in Whitehaven, Cumbria from 10th to 13th July. By exploring the physical, chemical and radiological properties of plutonium and the other actinides, the school provided an introduction to the 'Plutonium Futures – The Science 2012' conference, which was held in Cambridge the following week.

Forty-seven delegates from Europe, Russia, Japan and Korea attended the school and saw presentations by distinguished speakers from NNL, AWE, CEA, SUBATECH and the Universities of Manchester, Bristol and Edinburgh. The delegates were given an introduction to the nuclear fuel cycle, learned about reprocessing and chemical separations, actinide co-ordination chemistry, condensed matter physics, radiolysis and radiation chemistry, atomistic simulation techniques, the detection of actinide species and the practicalities of storing separated plutonium.

As well as lectures, the summer school also included some more interactive elements held at the University of Manchester's Dalton Cumbrian Facility, including the chemical analysis of irradiated polymers, exploring actinide chemistry using computational methods and developing strategies for the disposition of plutonium. The students also visited the NNL Central Laboratory at Sellafield and saw a live demonstration of the dissolution of a UO_2 pellet and the method of separation of uranium and plutonium from spent nuclear fuel used in the PUREX process.

THE PERIODIC TABLE OF VIDEOS

Periodic Videos on YouTube

NNL has been featured in the award winning Periodic Videos. Led by a team at The University of Nottingham the series of YouTube videos have a short and lively video clip for each element in the periodic table. They aim to communicate the excitement of science to a general audience and many of the videos contain live experiments. The highly successful videos have been viewed more than 15 million times on YouTube! Periodic Videos have been featured in both Science and Nature and have won many different awards.

NNL's PuMA lab was featured in the Plutonium, Americium and Neptunium videos that can be viewed at http://www.periodicvideos.com/index.htm.

PhD Award

Recently NNL employee *Zoe Maher* graduated from The University of Manchester with a PhD in Chemistry. Her research was carried out at NNL Central Lab and involved the study of actinides and colloids present in the historic storage ponds at Sellafield and how these species are removed during the SIXEP (Sellafield Ion-eXchange Effluent Plant) treatment process. The work was funded through the Royal Commission for the Exhibition of 1851 Industrial Fellowship, Sellafield Ltd Technical Directorate and SIXEP Technical. A number of journal articles describing the results are currently in preparation.

NNL in Europe

The NNL continue to play a lead role in several EU projects within the Seventh Framework Programme (FP7):

- **ACSEPT** – The ACSEPT (Actinide Recycling by Separation and Transmutation) project ran for four and a half years from 2008 until 2012. Funding was provided by the EU, Sellafield Ltd and by NDA through its Direct Research Portfolio (DRP). The project researched new ways to reduce the inventory of radioactive waste, thereby contributing to sustainable nuclear energy. NNL was a major project partner working alongside over 20 European laboratories and universities. The NNL's 'PuMA lab' was used to carry out experimental work for the ACSEPT project towards developing a GANEX (grouped actinide extraction) process. Whilst the separation of U and Pu is well established there remains a challenge to recover the remaining actinides particularly from the chemically similar lanthanides. The aim of GANEX is to extract all of the actinide species in solution into a solvent (*offering proliferation resistance*) and then selectively backwashing to produce a separate actinide product. In collaboration with researchers in Germany and France, work progressed from small scale batch reactions, in which the experimental variables were determined, to several rig trials in which the behaviour of the full separation process was studied and finally a hot test on irradiated fuel at the Institute of Transuranium Elements. www.acsept.org

- **ASGARD** – ASGARD (Advanced Fuels for Generation IV Reactors: Reprocessing and Dissolution) is a four year programme and work began in 2012; funding is provided by the EU, NNL and NDA. It focuses on advanced/novel nuclear fuel for Gen IV reactors focussing on their fabrication and respective reprocessing issues. ASGARD seeks integration between reactor, fuel and recycling communities and is an international effort of 16 institutions from 9 European countries. NNL's involvement is with the fabrication and reprocessing of carbide fuel. http://asgardproject.eu/

- **SACSESS** – Work on SACSESS (Safety of Actinide Separation Processes) began in March 2013. Among the different strategies studied to manage nuclear waste, partitioning and transmutation (P&T) allows a reduction of the amount, the radiotoxicity and the thermal power of wastes leading to optimal use of the geological repository sites. SACSESS will provide a structured framework to enhance the fuel cycle safety associated to P&T. By optimising the safety of both aqueous and pyro separation processes, it will allow the actinide recovery on sound scientific and technical basis. All these data will be integrated to optimise flowsheets and process operation conditions. SACSESS will be dedicated to safety and focus on the optimisation and improvement strategy on the basis of the existing systems.

- **CARBOWASTE** – This European collaborative research project 'Treatment and Disposal of Irradiated Graphite and other Carbonaceous Waste (CARBOWASTE)' commenced in 2008, and will complete in 2013. The aim of the project is to develop best practices in the retrieval, treatment and disposal of irradiated graphite, addressing both existing legacy waste as well as waste from graphite-based nuclear fuel resulting from a new generation of nuclear reactors. The consortium is led by Forschungszentrum, Juelich (FZJ) in Germany and involves 28 partners from Belgium, France, Germany, Italy, Lithuania, Netherlands, Romania, South Africa, Spain, Sweden and the United Kingdom. The National Nuclear Laboratory is leading the Integrated Waste Management Work Package. The Carbowaste project is building a harmonised 'tool box' of techniques, methodologies and best practices for decommissioning and waste management of irradiated graphite, that can be applied to the specific needs and conditions within a country and site. http://www.carbowaste.eu/

- **GoFastR** – GoFastR (Gas-cooled Fast Reactor) is a three year programme that began in 2010 and will conclude in 2013. Funding is provided by the EU and NNL through the Reactors and Fuels Signature Research Programme. The Gas-cooled Fast Reactor (GFR) is a Generation IV reactor design that is being developed in order to be safe, sustainable, economic and proliferation resistant. In particular, GFR could be capable of operating at very high temperatures (higher than other fast reactors) thus allowing for more efficient electricity generation and the supply of process heat for other applications such as hydrogen gas production. The GoFastR project has focused on the development of the designs for GFR and the ALLEGRO demonstrator reactor with contributions from 22 institutions across 9 European countries. NNL has contributed a strategic assessment of the potential impact of GFR in the fuel cycle, a fuel performance assessment of the MOX fuel proposed for the first lower temperature core of ALLEGRO and a review of advanced cladding materials for the subsequent higher temperature ALLEGRO cores. NNL's work for the project has now been completed.

AUTHORS' BIOGRAPHIES

Nassia Tzelepi has a MSc in Energy Systems and the Environment from the University of Strathclyde and a MBA with the Hellenic Open University. She has 13 years experience in the wider energy industry, 9 of which on nuclear graphite. Nassia's current role as Senior Graphite Specialist is to support the technical management of Magnox and AGR graphite work, with a focus on consistency, accuracy and quality across both customer work areas. Nassia is also involved in graphite waste management and treatment studies and is a Visiting Teaching Fellow in Nuclear Engineering at the University of Central Lancashire.

Paul Ramsay has work for the nuclear industry for 28 years determining material properties. Twelve years of engineering support for large scale sodium/water reaction rigs in support of the Fast Reactor programme at Dounreay, aimed at determining the best metal alloy able to withstand the effects of possible leaks which might occur in the steam generators. Paul develops facilities and techniques needed for measuring the effects of the extreme environment found within a nuclear reactor's core on the fuel elements, lately the focus has been specifically on the material from the graphite moderator core of the UK's Advanced Gas Reactors.

Martin Metcalfe is the National Nuclear Laboratory Senior Fellow for Graphite Technology. He has over 35 years experience in the nuclear industry, originally joining the CEGB after completing a PhD in physical chemistry at the University of Cambridge. He has specialised in graphite core safety case methodology, graphite core monitoring and surveillance, graphite material properties and graphite waste management. He has directed graphite research programmes for predecessor organisations and has directed the NNL strategy for graphite. He is internationally recognised as an expert in this field, being a founder member of the International Nuclear Graphite Specialist Meetings, a participant on the ASTM Manufactured Carbon and Graphite Products Committee and a member of the UK peer review Graphite Core Committee.

Glyn Rossiter is an internationally known expert in fuel rod thermo-mechanical behaviour, with 18 years experience working in the nuclear industry. His primary expertise is in light water reactor (LWR) fuel performance (including design and licensing of LWR fuel). Glyn also has experience in advanced gas-cooled reactor (AGR), fast reactor fuel performance and in LWR core thermal-hydraulics and he is the fuel performance technical lead for the NNL. He is also the UK fuels and materials technical lead in the OECD Halden Reactor Project. Glyn's other activities in the international fuel performance community include membership of the Nuclear Energy Agency (NEA) Expert Group on Reactor Fuel Performance (EGRFP) and of the World Nuclear Association (WNA) Fuel Technology Working Group (FTWG).

Ian Palmer is a Senior Scientist in Fuel Performance in the Nuclear and Reactor Physics team. He has over thirty years experience in the field of in-reactor fuel behaviour modelling, working mainly on the maintenance, development and validation of the ENIGMA code, the UK's principal tool for thermal reactor fuel design and licensing.

AUTHORS' BIOGRAPHIES

Robert Gregg has worked at the NNL/BNFL for 10 years in the advanced reactors team, after completing the 'Physics and Technology of nuclear reactors' MSc at the University of Birmingham. He has neutronically modelled several different reactor concepts ranging from PWRs to fast reactors. Recently, Robert has been working towards modelling future UK nuclear fuel cycles with the aim of assessing the impact these might have on future nuclear capacity, fuel fabrication and geological disposal of nuclear waste.

Robin Taylor (C.Chem., FRSC) is the National Nuclear Laboratory's Senior Fellow for Actinide Chemistry. Based at the NNL's Central Laboratory, he has led various R&D programmes in the fields of reprocessing of spent fuel and partitioning of minor actinides, including the NNL's contributions to the European Framework 7 projects - ACSEPT and SACSESS. He is a member of the OECD NEA Expert Group for Fuel Recycling Chemistry and in 2009 was presented the Bill Newton award from the Radiochemistry Group of the Royal Society for his work on "the behaviour of actinides in industrially relevant systems". Robin obtained a Ph.D. in radiochemistry from the University of Manchester and joined the Research and Development department at Sellafield in 1992.

Colin Gregson is a Senior Research Technologist based at the NNL'S Central Laboratory. He has been involved in R&D programmes from waste characterisation within legacy ponds (Corroded Magnox Sludge and soluble plutonium speciation) to the development of advanced reprocessing flowsheets for spent fuel incorporating minor actinide partitioning. Colin also provides technical support to both Magnox and Thorp reprocessing. Colin obtained a BSc(Hons) from UCLAN in 1993 and joined NNL in 2006 having previously work in the field of surfactant synthesis.

Mark Sarsfield (BSc, PhD, CChem) is an NNL Fellow in Actinide Chemistry and Honorary Visiting Research Fellow at the University of Manchester. Mark leads projects relating to the chemistry of the actinides for the European Space Agency, EU Framework VII (ASGARD), Nuclear Decommissioning Authority and Sellafield Ltd. He has 9 years experience in reprocessing chemistry supporting Magnox, THORP and Highly Active waste processing plants and is involved in research underpinning the safe storage of plutonium dioxide at Sellafield. Mark has co-authored over 40 publications in peer reviewed scientific journals.

Helen Steele has a Ph.D in quantum mechanics (QM), from the University of Manchester and has expertise in the calculation of actinide reactions and redox properties. She was awarded a Marie-Curie CEA-Eurotalents fellowshipin 2011 to study actinide redox couples and is currently a member of the LILA team on secondment at CEA-Marcoule. Helen supports a range of operations on Sellafield site through computer modelling techniques and has been with NNL for 7 years.

AUTHORS' BIOGRAPHIES

Susan Ortner is a Senior Consultant in the Reactor Chemistry and Materials Team. She has worked in the area of microstructural development and integrity of structural materials under thermal ageing and irradiation for 25 years, combining a variety of experimental techniques and modelling work. She is recognised internationally for her expertise in radiation damage and fracture modelling of reactor pressure vessel steels, and the associated development of embrittlement trend curves.

Jonathan Hyde, Chief Technology Officer for the Reactor and Operations Support business, is a Senior Visiting Fellow at the University of Oxford and a Visiting Professor for the Dalton Nuclear Institute at the University of Manchester. His current research interests focus on characterising and developing mechanistic understanding of radiation damage in materials. This includes active involvement in Research and Development (R&D), strategic development and management of R&D programmes, consultancy, expert review and line management activities. He is the author or co-author of two book chapters and more than 70 peer reviewed articles.

Kat Lennox is a Research Technologist who graduated with a first class joint honours Masters degree in Maths and Physics from The University of Manchester. During her final year, Kat completed two Masters projects; one relating to the NNL's RadBall technology and the second relating to criticality safety. Directly after graduating Kat joined the NNL in September 2010 as a graduate in the Criticality Safety team. Kat has now moved full time into the Instrumentation and in-situ analysis team working primarily on in-situ analysis.

Steve Stanley is an NNL Business Manager and Intellectual Property Manager. He is responsible for the invention and development of the NNL's RadBall® technology as well as the RadLine™ radiation detector. He has won a number of awards including the IChemE British Young Engineer Award (2008), the IChemE Innovation and Excellence in Health and Safety Award (2008), the British Young Engineer of the Year Awards (2006) as well as two NNL Internal Innovation awards (2006/2007). He is also a Fellow of the Institute of Chemical Engineering (FIChemE) and is both a Chartered Engineer (CEng) and Chartered Scientist (CSci). He graduated with Masters Degree in Chemical Engineering (MEng) from The University of Manchester and went on to undertake a Masters of Philosophy (MPhil) and a PhD specialising in the use of tomographic imaging techniques to study industrial crystallisation. He has over 75 publications in peer reviewed journals, conference proceedings and industry magazines.

BOOK SECTIONS [1-2]

(1) F.P.L. Andrieux; C. Boxall; R.J. Taylor In *Application of Thermodynamics to Biological and Materials Science*; Tadashi, M., Ed.; InTech: Rijeka, Croatia, p 441, (2011). ISBN 978 953 307 980 6.

(2) S. Vyas; S.L. Owens; M. Bankhead In *Industrial applications of Molecular Simulations*; Meunier, M., Ed.; CRC Press, (2011). ISBN 978 1 4398 6101 1.

JOURNAL ARTICLES [3-33]

(3) M. Angus; S. Palethorpe; C. Scales, "Encapsulation options for decommissioning wastes" *Nuclear Future, 7*, 35, (2011).

(4) Y. Bai; N.C. Collier; N.B. Milestone; C.H. Yang, "The potential for using slags activated with near neutral salts as immobilisation matrices for nuclear wastes containing reactive metals" *Journal of Nuclear Materials, 413*, 183, (2011).

(5) P. Blowers; J. Caborn; T. Dell; T. Gingell; A. Harms; S. Long; D. Sleep; C. Stewart; J. Walker; P.E. Warwick, "Determination of carbon-14 in environmental level, solid reference materials" *Applied Radiation and Isotopes, 69*, 1323, (2011).

(6) J.J. Bommer; M. Papaspiliou; W. Price, "Earthquake response spectra for seismic design of nuclear power plants in the UK" *Nuclear Engineering and Design, 241*, 968, (2011).

(7) S. Bourg; C. Hill; C. Caravaca; C. Rhodes; C. Ekberg; R. Taylor; A. Geist; G. Modolo; L. Cassayre; R. Malmbeck; M. Harrison; G. de Angelis; A. Espartero; S. Bouvet; N. Ouvrier, "ACSEPT— Partitioning technologies and actinide science: Towards pilot facilities in Europe" *Nuclear Engineering and Design, 241*, 3427, (2011).

(8) A.J. Connelly; N.C. Hyatt; K.P. Travis; R.J. Hand; E.R. Maddrell, "Predicting the preference for charge compensation in silicate glasses" *Physics and Chemistry of Glasses-European Journal of Glass Science and Technology Part B, 52*, 64, (2011).

(9) A.J. Connelly; N.C. Hyatt; K.P. Travis; R.J. Hand; E.R. Maddrell; R.J. Short, "The structural role of Zr within alkali borosilicate glasses for nuclear waste immobilisation" *Journal of Non-Crystalline Solids, 357*, 1647, (2011).

(10) A.J. Connelly; K.P. Travis; R.J. Hand; N.C. Hyatt; E. Maddrell, "Composition-Structure Relationships in Simplified Nuclear Waste Glasses: 2. The Effect of ZrO2 Additions" *Journal of the American Ceramic Society, 94*, 78, (2011).

(11) A.J. Connelly; K.P. Travis; R.J. Hand; N.C. Hyatt; E. Maddrell, "Composition-Structure Relationships in Simplified Nuclear Waste Glasses: 1. Mixed Alkali Borosilicate Glasses" *Journal of the American Ceramic Society, 94*, 92, (2011).

(12) J. Deshon; D. Hussey; B. Kendrick; J. McGurk; J. Secker; M. Short, "Pressurized Water Reactor Fuel Crud and Corrosion Modeling" *Jom, 63*, 68, (2011).

(13) C.R. Gregson; D.T. Goddard; M.J. Sarsfield; R.J. Taylor, "Combined electron microscopy and vibrational spectroscopy study of corroded Magnox sludge from a legacy spent nuclear fuel storage pond" *Journal of Nuclear Materials, 412*, 145, (2011).

(14) C.R. Gregson; J.J. Hastings; H.E. Sims; H.M. Steele; R.J. , "Characterisation of plutonium species in alkaline liquors sampled from a UK legacy nuclear fuel storage pond" *Analytical Methods, 3*, 1957, (2011).

(15) J.N. Haque; T. Mahmud; K.J. Roberts; J.K. Liang; G. White; D. Wilkinson; D. Rhodes, "Free-Surface Turbulent Flow Induced by a Rushton Turbine in an Unbaffled Dish-Bottom Stirred Tank Reactor: LDV Measurements and CFD Simulations" *Canadian Journal of Chemical Engineering, 89*, 745, (2011).

(16) G.L. Hill; E. Bailey; M.C. Stennett; N.C. Hyatt; E.M. Maddrell; P.F. McMillan; J.A. Hriljac, "High-Pressure and -Temperature Ion Exchange of Aluminosilicate and Gallosilicate Natrolite" *Journal of the American Chemical Society, 133*, 13883, (2011).

(17) J.M. Hyde; M.G. Burke; B. Gault; D.W. Saxey; P. Styman; K.B. Wilford; T.J. Williams, "Atom probe tomography of reactor pressure vessel steels: An analysis of data integrity" *Ultramicroscopy,* **111**, 676, (2011).

(18) J.M. Hyde; E.A. Marquis; K.B. Wilford; T.J. Williams, "A sensitivity analysis of the maximum separation method for the characterisation of solute clusters" *Ultramicroscopy,* **111**, 440, (2011).

(19) J.M. Hyde; G. Sha; E.A. Marquis; A. Morley; K.B. Wilford; T.J. Williams, "A comparison of the structure of solute clusters formed during thermal ageing and irradiation" *Ultramicroscopy,* **111**, 664, (2011).

(20) M.J. Jones; L.J. Butchins; J.M. Charnock; R.A.D. Pattrick; J.S. Small; D.J. Vaughan; P.L. Wincott; F.R. Livens, "Reactions of radium and barium with the surfaces of carbonate minerals" *Applied Geochemistry,* **26**, 1231, (2011).

(21) A.J. Koning; E. Bauge; C.J. Dean; E. Dupont; U. Fischer; R.A. Forrest; R. Jacqmin; H. Leeb; M.A. Kellett; R.W. Mills; C. Nordborg; M. Pescarini; Y. Rugama; P. Rullhusen, "Status of the JEFF Nuclear Data Library" *Journal of the Korean Physical Society,* **59**, 1057, (2011).

(22) S.R. Ortner, "Comparison between particle cracking criteria in models for the fracture of steels" *Fatigue & Fracture of Engineering Materials & Structures,* **34**, 956, (2011).

(23) S.R. Ortner; K.S. Lee; A.H. Sherry, "The effect of a residual stress field on fracture initiation in RPV steel" *Fatigue & Fracture of Engineering Materials & Structures,* **34**, 945, (2011).

(24) S.A. Parry; L. O'Brien; A.S. Fellerman; C.J. Eaves; N.B. Milestone; N.D. Bryan; F.R. Livens, "Plutonium behaviour in nuclear fuel storage pond effluents" *Energy & Environmental Science,* **4**, 1457, (2011).

(25) D.H. Phillips; G. Sinnathamby; M.I. Russell; C. Anderson; A. Paksy, "Mineralogy of selected geological deposits from the United Kingdom and the Republic of Ireland as possible capping material for low-level radioactive waste disposal facilities" *Applied Clay Science,* **53**, 395, (2011).

(26) M. Preuss; P. Frankel; S. Lozano-Perez; D. Hudson; P. E.; N. Ni; J. Wei; C. English; S. Storer; K. Chong; M. Fitzpatrick; P. Wang; J. Smith; C. Grovenor; G. Smith; J. Sykes; B. Cottis; S. Lyon; L. Hallstadius; B. Comstock; A. Ambard; M. Blat-Yrieix, " Studies Regarding Corrosion Mechanisms in Zirconium Alloys" *Journal of ASTM International* **8**, 1, (2011).

(27) B.J. Riley; P.R. Hrma; J.D. Vienna; M.J. Schweiger; C.P. Rodriguez; J.V. Crum; J.B. Lang; J.C. Marra; F.C. Johnson; D.K. Peeler; C. Leonelli; A.M. Ferrari; I. Lancellotti; J.-L. Dussossoy; R.J. Hand; J.M. Schofield; A.J. Connelly; R. Short; M.T. Harrison, "The Liquidus Temperature of Nuclear Waste Glasses: An International Round-Robin Study" *International Journal of Applied Glass Science,* **2**, 321, (2011).

(28) G. Rossiter, "Development of the ENIGMA Fuel Performance Code for Whole Core Analysis and Dry Storage Assessments" *Nuclear Engineering and Technology,* **43**, 489, (2011).

(29) B.E. Rotter; D.A. Barry; J.I. Gerhard; J.S. Small, "Modeling the effectiveness of U(VI) biomineralization in dual-porosity porous media" *Journal of Hydrology,* **402**, 14, (2011).

(30) M.J.D. Rushton; R.W. Grimes; S.L. Owens, "Partial ordering of glass networks adjacent to simulated glass-crystal interfaces" *Journal of Non-Crystalline Solids,* **357**, 3278, (2011).

(31) M.J. Sarsfield; H.E. Sims; R.J. Taylor, "Modelling Np(IV) Solvent Extraction between 30% Tri-Butyl Phosphate and Nitric Acid in the Presence of Simple Hydroxamic Acids" *Solvent Extraction and Ion Exchange,* **29**, 49, (2011).

(32) R.J. Taylor, "Advanced separation processes for actinide recycling" *The Chemical Engineer,* **41-43**, 844, (2011).

(33) C.A. Williams; J.M. Hyde; G.D.W. Smith; E.A. Marquis, "Effects of heavy-ion irradiation on solute segregation to dislocations in oxide-dispersion-strengthened Eurofer 97 steel" *Journal of Nuclear Materials,* **412**, 100, (2011).

RoSPA
2011

Winner
RESEARCH & DEVELOPMENT
Sector Award

LLOYD'S REGISTER QUALITY ASSURANCE · ISO9001

LLOYD'S REGISTER QUALITY ASSURANCE · ISO 14001

LLOYD'S REGISTER QUALITY ASSURANCE · ISO/IEC27001

5th Floor
Chadwick House
Warrington Road
Birchwood Park
Warrington
WA3 6AE

T. +44 (0) 1925 289800
E. customers@nnl.co.uk

W. www.nnl.co.uk

@UKNNL

NATIONAL NUCLEAR
LABORATORY